Sources, degassing and contamination of CO_2, H_2O, He, Ne and Ar in basaltic glasses from Kolbeinsey Ridge, North Atlantic

Colin G. Macpherson[1*,2], David R. Hilton[2], Dieter F. Mertz[3] and Tibor J. Dunai[4]

[1]Department of Earth Sciences, University of Durham, Durham, DH1 3LE, UK.

[2]Geosciences Research Division, Scripps Institution of Oceanography, La Jolla, CA 92093-0244 USA

[3]Johannes Gutenberg-Universitat, Institut fur Geowissenschaften, 55099 Mainz, Germany

[4]Vrije Universiteit, De Boelelaan 1085, 1081 HV Amsterdam, The Netherlands

* Corresponding author:
colin.macpherson@durham.ac.uk
Tel: +44 (0)191 334 2283
Fax: +44 (0)191 334 2301

Resubmitted to *Geochimica et Cosmochimica Acta* 27 July 2005

ABSTRACT

New volatile data (CO_2, H_2O, He, Ne and Ar) are presented for 24 submarine basaltic glasses from the Kolbeinsey Ridge, Tjörnes Fracture Zone and Mohns Ridge, North Atlantic. Low CO_2 and He contents indicate that magmas were strongly outgassed with the extent of degassing increasing towards the south, as expected from shallower ridge depths. Ne and Ar are significantly more abundant in the southernmost glasses than predicted for degassed melt. The strong atmospheric isotopic signal associated with this excess Ne and Ar suggests syn- or post-eruptive contamination by air. Degassing, by itself, cannot generate the large variations in $\delta^{13}C$ values of dissolved CO_2 or coupled CO_2 – Ar variations. This suggests that $\delta^{13}C$ values were was also affected by some other processes, most probably melt – crust interaction. Modelling indicates that degassing had a negligible influence on water due to its higher solubility in basaltic melt than the other volatiles. Low H_2O contents in the glasses reflect melting of a mantle source that is not water-rich relative to the source of N-MORB.

Prior to eruption Kolbeinsey Ridge melts contained ~ 400 ppm CO_2 with $\delta^{13}C$ of -6‰, 0.1 to 0.35 wt.% H_2O, $^3He/^4He$ ~ 11 R_A, and $CO_2/^3He$ of ~ 2×10^9. We model restored volatile characteristics and find homogeneous compositions in the source of Kolbeinsey Ridge magmas. Relative to the MORB-source, He and Ne are mildly fractionated while the $^{40}Ar/^{36}Ar$ may be low. The $^3He/^4He$ ratios in Tjörnes Fracture Zone glasses are slightly higher (13.6 R_A) than on Kolbeinsey Ridge, suggesting a greater contribution of Icelandic mantle from the south, but the lack of $^3He/^4He$ variation along the Kolbeinsey Ridge is inconsistent with active dispersal of Icelandic mantle beyond the Tjörnes Fracture Zone.

1. INTRODUCTION

A gas phase is usually present in submarine glasses because volatile components (particularly CO_2) are relatively insoluble in basaltic magma; consequently, volatiles are effectively transferred from melt to vapour (exsolved) during magma ascent. The subsequent record of volatile partitioning between vapour and melt can be employed to establish a number of intrinsic melt properties, such as storage

depths and relative transportation rates through the crust (Dixon et al., 1988; Macpherson and Mattey, 1994). In addition, volatile components can be exploited as tracers of the nature and development of mantle reservoirs. In this respect, much emphasis is placed on identifying differences in the volatile characteristics of basalts erupted at mid-ocean ridges and ocean islands (Graham, 2002).

Iceland is particularly relevant to volatile studies because the Mid-Atlantic Ridge rises above sea level and allows direct sampling of magmatic gases. Prior work on Iceland has established that magmatic He and Ne (Mamyrin et al., 1972; Condomines et al., 1983; Kurz et al., 1985; Sano et al., 1985; Hilton et al., 1990; Burnard et al., 1994; Breddam et al., 2000; Dixon et al., 2000; Moreira et al., 2001), and possibly Ar (Trieloff et al., 2000), are isotopically distinct from typical mid-ocean ridge basalt (MORB). Icelandic lavas may also be water-rich compared to the majority of MORB (Nichols et al., 2002). These findings suggest that the source of Icelandic magmatism is distinct from those supplying most of the world's spreading centres. This places important constraints on the nature and origin of the thermal and/or chemical anomaly thought to cause the high magma flux through and around Iceland.

In this study, we present new concentration and isotopic data for CO_2, H_2O, He, Ne and Ar in glasses from Kolbeinsey Ridge and the Tjörnes Fracture Zone. The Kolbeinsey Ridge accommodates North Atlantic spreading immediately north of Iceland and lies in shallow water (<1250m). The volatile record of its magmatic rocks has received relatively little attention compared to the Reykjanes Ridge, south of Iceland (Poreda and di Brozolo, 1984; Poreda et al., 1986; Botz et al., 1999; Schilling et al., 1999). The Tjörnes Fracture Zone displaces the Kolbeinsey Ridge from active rifting in northern Iceland and comprises a series of sub-parallel NNW-striking grabens with accompanying magmatism (Gudmundsson, 1995; Schilling et al., 1999). This contribution has two primary aims. The first is to identify and quantify the processes affecting magmas erupted in relatively shallow submarine settings. Deep (>2500 m) submarine glasses preserve a range of degassing states so provide a valuable record of primitive magmatic volatiles and the means by which they are lost from basaltic magma. However, dense sampling of shallow submarine sites is rare. The new dataset bridges the gap between sampling sites in the deep submarine environment and those on land (such

as Iceland) thereby providing an opportunity to study those processes affecting volatiles as basaltic melt is transported through relatively thick oceanic crust. The second aim is to determine the nature of primitive volatile components along the Kolbeinsey Ridge and to compare these with Iceland, where distinctive volatile signatures are a conspicuous feature of subaerial magmatism. From this perspective, the new dataset provides an important complement studies of the Reykjanes Ridge and the Mid-Atlantic Ridge south of Iceland (Kurz et al., 1982 and 1985; Condomines et al., 1983; Poreda and di Brozolo, 1984; Poreda et al., 1986; Poreda et al., 1992; Michael and Cornell, 1998; Harrison et al., 1999; Hilton et al., 1999 and 2000; Nichols et al., 2002).

2. GEOLOGICAL SETTING AND SAMPLES

Kolbeinsey Ridge is located immediately to the north of Iceland and is a slow-spreading section of the Mid-Atlantic Ridge (half spreading rate ~1cm/year; Vogt, 1983) that initiated at approximately 22Ma when the Aegir Ridge, to the east, became inactive (Talwani and Eldholm, 1977; Vogt et al., 1980). It is offset from the Iceland axial rift by the Tjörnes Fracture Zone (~ 67°N) and extends to Eggvin Bank at ~ 71°N, adjacent to the Jan Mayen Fracture Zone (Fig. 1). The ridge is segmented into Northern and Southern sections by the Spar Offset Zone at 69°N (Fig. 1a; Applegate, 1997). Adjacent to the Tjörnes Fracture Zone, the ridge crest is approximately 100m below sea level and plunges to ~1km depth at the Spar Offset. North of the Spar Offset, the ridge reaches depths of 1250m before shoaling to 300m at Eggvin Bank (Fig. 1). The shallow water depths, compared to most spreading centres, are the result of greater crustal thickness (Kodaira et al., 1998). Abundant fresh glass has been recovered from all parts of the ridge indicating that volcanism is active along most of its length (Devey et al., 1994).

Major volatile (CO_2 and H_2O) and light noble gas (He, Ne and Ar) data were obtained for 23 glasses collected from the Southern and Northern segments of the Kolbeinsey Ridge and from the Tjörnes Fracture Zone. Details of collection programmes can be found in Mertz et al (1991) and Devey et al. (1994). Table 1 gives the locations and collection depths of the glasses, which are all tholeiitic basalts. MgO contents range from 6 to 10 wt.% and SiO_2 ranges from 48.5 wt.% to 51 wt.%. Kolbeinsey Ridge has erupted some of the most incompatible trace element depleted mid-

ocean ridge basalts (Mertz et al., 1991; Devey et al., 1994; Mertz unpublished data). Fractionation corrected incompatible element indicators, such as $Na_{8.0}$, are amongst the lowest of any MORB; however, trace element ratios display more significant variation, which has been attributed to dynamic melting (Devey et al., 1994). The glasses display some variation in $^{87}Sr/^{86}Sr$ and $^{143}Nd/^{144}Nd$, and relatively little variation in Pb isotopes (Mertz et al. 1991; Mertz and Haase, 1997), although a more recent study by Thirlwall et al. (2004) suggests that the Sr and Nd isotope variation observed along the Kolsbeinsey Ridge may be less than originally determined. A single basaltic glass from 2200 mbsl on the Mohns Ridge (at 72°N) was also analysed.

3. ANALYTICAL METHODS

----------can be small text ----------

Glass chips, free of phenocrysts and visible signs of alteration, were selected using a binocular microscope. These were ultrasonically agitated in a 50:50 mixture of acetone and methanol to remove alteration material and adhering matrix. The CO_2, H_2O and light noble gases were characterised using three experimental techniques. Further visual inspection of the glass was conducted prior to each experiment to ensure the cleanest material was selected.

The concentrations of CO_2 and H_2O and the $^{13}C/^{12}C$ of carbon were determined on volatiles released by stepped heating (Macpherson et al., 1999). Pre-cleaning and low temperature combustion (400°C and 600°C) removed secondary surface deposits introduced after eruption. Pyrolysis in 100°C increments allowed sequential extraction of CO_2 from bubbles (700°C to 900°C) and CO_2 dissolved in glass (900°C to1200°C). CO_2 and H_2O were isolated cryogenically. CO_2 yields were measured with a Baratron® capacitance manometer and the CO_2 was trapped in a quartz glass tube for later isotopic analysis. Low yield steps were combined with subsequent step(s) for isotopic analysis. $\delta^{13}C$ values, reported relative to V-PDB, were measured with a VG PRISM mass spectrometer. All water accumulated from the 600°C step onward provided the H_2O sample (Macpherson et al. 1999). Water was reduced over Zn and yields were measured with a VG PRISM mass spectrometer, to ±0.10 wt.% (1σ), by comparison to H_2^+ peaks generated from

known volumes of H_2O . All CO_2, H_2O and $\delta^{13}C$ data have been corrected for the presence of a procedural blank.

Approximately 500 mg of glass fragments, 1 to 5mm in diameter, were selected for measurement of He concentrations ([He]) and $^3He/^4He$ using a VG5400 noble gas mass spectrometer at the Vrije Universiteit, Amsterdam. Glasses were crushed on-line in a custom-built crusher similar to that described by Stuart et al. (1994). Each sample was loaded into a ~1 cm deep stainless-steel container in three layers separated by four stainless-steel discs to maximise the surface area in contact with the crusher. This markedly increased crushing efficiency compared to single bulk loading of grains. The container was then placed in a machined block, sealed on a CF35 flange and the system was pumped to UHV and heated to ~100°C overnight. Three crushers, arranged in series, were loaded together and a hydraulic press (operated to 2 tons pressure) was used to crush the samples. Released gas was expanded into an all-metal preparation line and then exposed to active gas getters (a Ti-sponge fingers held a 800°C and 400°C followed by a Zr-Al SAES® getter), activated charcoal at -196°C, to absorb heavy noble gases, and then a liquid-helium cooled refrigerator trap held at 34K, to separate He from Ne. A fixed machine resolution of 600 ensured complete separation of ^3He from HD. ^3He measurements were made in analogue mode using a Johnston MM-1 electron multiplier and the peak was frequently re-centred during the course of each analysis to correct for drift. ^4He was measured on a conventional Faraday collector. All $^3He/^4He$ ratios were calculated relative to an in-house standard gas (Krusivik, Iceland = 14 R_A) run immediately following sample runs at approximately the same (flight tube) He partial pressure. Crusher blanks were routinely ~ 1×10^{-10} cm^3STP ^4He. Concentrations were derived from peak height comparison to standards (admitted by calibrated pipette) with sample weights calculated using the fraction of sample passing through a 100 µm sieve.

Ne and Ar concentrations and isotope ratios and He/Ar ratios were determined by stepped heating at the Scripps Institution of Oceanography using a modified VG5400 equipped with a Daly photo-sintillator (Craig et al., 1993). Samples were wrapped in Al foil and loaded into the all-metal preparation system. A water-cooled, resistance furnace, with molybdenum crucible, was calibrated up to 1650°C and baked repeatedly to achieve required blank levels. Data have been corrected for

the presence of a procedural blank. Due to low intrinsic gas contents of some samples (and sample sizes) the blank contribution was relatively large but less than 25% in most cases. For larger contributions up to 60% results are listed in italics in Table 2. As a result of these corrections some samples have relatively large uncertainties, notably in their measured Ne isotope ratios. However, because of the reproducibility of the blank, we are confident that the data accurately reflect the Ne and Ar characteristics of the glasses. Typical blanks, which include Al foil, were 1×10^{-12} cm^3STP ^{22}Ne and 4×10^{-9} cm^3STP ^{40}Ar at 800°C, and 1×10^{-12} cm^3STP ^{22}Ne and 3.5×10^{-9} cm^3STP ^{40}Ar at 1200°C. Isotope ratios of the blanks were within error of atmospheric values. An initial heating step at 600°C was used to remove atmospheric gases contained in surface deposits or absorbed into the outer surface of the glass (Sarda et al., 1985, 1988; Marty and Zimmermann, 1999). Fusion at 1400°C (after extraction) ensured the crucible was purged before receiving a new sample. Extractions at 800°C and 1200°C were performed in an attempt to resolve vesicle and dissolved components, respectively (see below). Extracted gases were exposed, in turn, to two Ti-sponges that were cooled from 750°C to 450°C after which Ar was trapped onto a stainless-steel frit at 77K. The remaining gas was exposed to a SAES getter, and then He and Ne were trapped on activated charcoal cooled to <14K. Heating the charcoal to 36K retained Ne, while He was released for measurement, and subsequent heating to 95K released Ne for measurement. Finally, Ar was exposed to the SAES getter before inlet to the mass spectrometer. Isotope ratios and gas abundances were measured using a peak-jumping routine, developed in-house, between an axial Faraday collector and off-axis Daly photo-multiplier, with peak heights extrapolated to the time of inlet. An air standard was used to monitor detector sensitivities and mass discrimination. During He and Ne analyses, a stainless steel frit in the source was chilled to 77K. Procedures employed to correct for interferences by Ar^{++} and CO_2^{++} during Ne analyses are similar to those described by Niedermann et al. (1993). Ar was allowed to equilibrate in the mass spectrometer for 10 minutes prior to analysis to eliminate potential hydrocarbon interference over the m/e range 35 to 38.

We regard dissolved volatiles as the whole complement of H_2O, the high temperature CO_2 (as discussed above) and Ar recovered at 1200°C. Our approach did not allow recovery of dissolved He, and effective sampling of dissolved Ne was unlikely. Vesicle gas is the He released by crushing

and the CO_2 and Ar data obtained at the intermediate stages of stepped heating experiments. Determination of inter-volatile ratios can be compromised when there are significant differences in the way samples are analysed and pre-treated, or as a result of heterogeneous vesicle preservation and distribution (Burnard et al., 2004). This is not a problem for He/Ar which was measured directly on the same split. With the exception of one sample (Pol22Ds-2a is very Ar-rich with atmospheric $^{40}Ar/^{36}Ar$) there is a broad, positive correlation between the amount of Ar and CO_2 recovered from vesicles by stepped heating (Tables 1 and 2). Since the two splits experienced similar heating profiles this suggests similar vesicle distributions. A similar broad, positive correlation between the abundance of vesicle CO_2 and He determined by crushing (Table 1) would not be expected if there was a significant difference in vesicle distribution between splits used in different experiments. All ratios between different vesicle gases have been calculated as molar ratios.

----------end small text ----------

4. RESULTS

4.1 Carbon

Stepped heating results are listed in Appendix 1 while the concentration and $\delta^{13}C$ of dissolved and vesicle CO_2 are listed in Table 1. Dissolved CO_2 concentrations range from 16 ppm to 162 ppm and so are at the lower end of the range previously determined for mid-ocean ridges (Dixon and Stolper, 1995 and references therein), and are higher and more variable in glasses from the North Kolbeinsey Ridge than shallower eruption sites close to Iceland (Fig. 2c). Concentrations of vesicle CO_2 are, with two exceptions (samples Pol 21848 and Pol 21856-3), lower than dissolved CO_2 concentrations (Fig. 2c). Some CO_2 extractions used relatively small chips (<2mm diameter) and, since larger vesicles contain the larger fraction of vesicle gas (Sarda and Graham, 1990), the samples may have been too small to represent the whole vesicle population. However, there was no evidence for broken large vesicles in any of the chips used. Furthermore, the number of chips processed in each experiment is unrelated to the volume of vesicle gas or the fraction of the total CO_2 residing in vesicles. The low concentration of vesicle gas suggests that much of the vesicle component was removed from magmas before quenching to glass.

$\delta^{13}C$ values vary widely, from –6.9‰ to –24.0‰ in the dissolved CO_2 and from –3.4‰ to –33.2‰ in vesicles (Table 1). These ranges are large compared to previous studies of spreading centre glasses (Exley et al., 1986; Mattey et al., 1989; Macpherson and Mattey, 1994; Pineau and Javoy, 1994). There is no simple relationship between $\delta^{13}C$ and latitude but the spread in $\delta^{13}C$ values of dissolved CO_2 increases towards Iceland, where the lowest values occur, while vesicle gases have more variable $\delta^{13}C$ within each segment (Fig. 2d).

4.2 Water

H_2O concentrations range from 0.10 to 0.33 wt.% (±0.10%; Table 1). Although the lower end of this range is at the limit of resolution, the important conclusion is that water concentrations are low, lying within the range reported for MORB (Michael, 1995) and are similar to or lower than previous determinations in Kolbeinsey Ridge glasses (Poreda et al., 1986). Water concentrations also lie at the lower end of the range determined for Iceland and the Reykjanes Ridge (Nichols et al., 2002). Unlike the Reykjanes Ridge, however, there is no relationship between H_2O content and either latitude or depth (Fig. 2b).

4.3 Helium

He concentrations range from 5 to 4623 x 10^{-9} cm^3STP/g and are generally lower in glasses erupted closer to Iceland. Low [He] occur throughout Tjörnes Fracture Zone and Kolbeinsey Ridge but the range increases to the north (Fig. 2e). Concentrations are low with respect to most N-MORB (90% of which have [He] > 1000 x 10^{-9} cm^3STP/g; Macpherson et al., 1998), as expected for eruption in shallow water (Carroll and Webster, 1994), and decrease from the Northern Kolbeinsey Ridge, through the South Kolbeinsey Ridge to the Tjörnes Fracture Zone (Fig. 2e). The Mohns Ridge glass also has low [He] compared to MORB.

Most glasses erupted between Iceland and the Jan Mayen Fracture zone display $^3He/^4He$ significantly greater than typical MORB (~ 8 ± 1 R_A (Graham, 2002), where R_A = $^3He/^4He$ of air). The highest $^3He/^4He$ values (~14 R_A) are found in the Tjörnes Fracture Zone, closest to Iceland (Fig. 2f). One glass (Pol21847) from the Northern Kolbeinsey Ridge possesses lower $^3He/^4He$ similar to N-MORB. The remaining North and South Kolbeinsey Ridge data are characterised by

remarkably constant $^3He/^4He$ (11.1 R_A ±0.9, n = 16). There is no change in $^3He/^4He$ associated with the Spar Offset (~ 69°N). Combining the new data with results from Schilling et al. (1999), with the exception of two of their glasses from very close to the Jan Mayen Fracture Zone, gives an overall mean $^3He/^4He$ of 11.0 R_A, ±0.9 (n = 29) for Kolbeinsey Ridge. This is slightly higher than ratios obtained for hydrothermal vent fluids from the southern end of the ridge (Botz et al., 1999). The single Mohns Ridge glass has a $^3He/^4He$ value of 7.0 R_A and falls well within the range of values previously shown to characterise the southern part of this segment of the Mid-Atlantic Ridge (Fig. 2f). The $^3He/^4He$ anomaly associated with Iceland extends to the most northerly Kolbeinsey Ridge site sampled in this work (70.6°N) and does not show a steady decrease with latitude as previously reported (Schilling et al., 1999). Rather, the highest ratios are found in the Tjörnes Fracture Zone but $^3He/^4He$ varies little along the length of the Kolbeinsey Ridge itself. At 70.6°N, close to the Jan Mayen Fracture Zone, there is a major discontinuity in the He profile. North of this discontinuity $^3He/^4He$ drops abruptly to ≤ 8 R_A (Fig. 2f).

4.4 Neon

Ne concentrations ([Ne]) and isotope ratios were obtained for 800°C and 1200°C steps (Table 2). At 1200°C [Ne] ranges from 26 to 883 x 10^{-12} cm^3STP/g and all isotope ratios lie within error of air. Since Ne is thought to be relatively mobile over the timescales of analysis at these temperatures (Jambon et al. 1986) it is likely that, at least some, magmatic Ne is removed from the melt phase before 1200°C is reached. Therefore, we focus mainly on the 800°C data.

The 800°C release of stepped heating experiments appears to provide a better sample of magmatic Ne in basaltic glasses (*c.f.* Hiyagon et al., 1992). At this temperature there is a wide range in [Ne] - from 22 to 6057 x 10^{-12} cm^3STP/g. Two aspects of this range are particularly striking. First, the higher end is comparable to [Ne] in many ocean ridge glasses (Graham, 2002). This is unexpected since the low solubility of Ne, with respect to CO_2 or He (Carroll and Webster, 1994), suggests that these North Atlantic Ridge glasses should have lost most of their intrinsic Ne. Second, the lowest [Ne] values are not in glasses from the shallowest depths; if anything, [Ne] increases on

shallower ridge sections (Fig. 2g), in contrast to the CO_2 and He data, suggesting that degassing is not the only process that has affected Ne.

Ne isotope ratios in the majority of 800°C releases are close to atmospheric values (Table 2). This result is similar to that obtained by Poreda and di Brozolo (1984) for a suite of seven glasses from the Kolbeinsey and Mohns Ridges. $^{20}Ne/^{22}Ne$ ratios distinct from atmosphere occur in the Ne-poor glasses from the North Kolbeinsey Ridge (Fig. 2h) and the same is true for $^{21}Ne/^{22}Ne$ (Table 2). In turn, this suggests that the excess Ne in the southernmost samples has an atmospheric origin.

4.5 Argon

Ar diffusion in basaltic glass is not significant over the timescale of the heating steps used in this study (Jambon et al., 1986). Therefore, the 800°C and 1200°C Ar releases are interpreted in the same way as the intermediate and high temperature fractions observed during CO_2 extraction *i.e.* as originating from vesicles and glass, respectively. The Ar concentrations ([Ar]) from vesicles vary from 18 to 4903 x 10^{-9} cm^3STP/g (Table 2). The highest concentrations are well within the range found at other spreading centres but the majority of Kolbeinsey Ridge glasses contain significantly less Ar than MORB (see Graham, 2002). Dissolved [Ar] varies from 15 to 801 x 10^{-9} cm^3STP/g. Ar can be likened to Ne in that glasses from the southernmost, shallow eruption sites contain significantly more gas than those from deeper sites on the South Kolbeinsey Ridge. Unlike Ne, Ar is also more abundant in some of the deeper sites on the Northern Kolbeinsey Ridge (Fig. 2i).

There is strong evidence that the glasses contain atmospheric Ar, as indicated by $^{40}Ar/^{36}Ar$. For both fractions, the lowest $^{40}Ar/^{36}Ar$ is close to the atmospheric ratio and these ratios become more common close to Iceland (Fig. 2j). The highest $^{40}Ar/^{36}Ar$ (3,667 in vesicles and 5,160 in the dissolved component) occur on the North Kolbeinsey Ridge, but are considerably lower than postulated for the MORB source ($\geq$ 40,000; Burnard et al., 1997). There is a wide range in $^4He/^{40}Ar^*$ ($^{40}Ar^*$ is the ^{40}Ar content corrected for the presence of atmospheric Ar) consistent with variable, fractional outgassing (Marty and Zimmerman, 1999). A single instance of $^4He/^{40}Ar^* < 1$ occurs on each segment, but $^4He/^{40}Ar^*$ generally increases from north to south (Table 2).

5. DISCUSSION

5.1 Dissolved Gases

5.1.1 Volatile Saturation of Kolbeinsey Ridge Magmas

Degassing of basaltic magmas occurs through formation of a gas phase dominated by the major volatiles CO_2 and H_2O. Other volatile components, principally the noble gases, are not sufficiently abundant in basic magmas to become saturated and so will partition between the melt and gas formed by the major volatiles. Polybaric degassing occurs as pressure decreases when magma is transported towards the surface. In submarine basalts, the water column above the eruption site provides the final confining pressure when magma is quenched. Therefore, dissolved major volatile contents should correlate positively with eruption pressure, as observed in glasses from some submarine environments e.g. Puna Ridge, Kilauea (Fig. 3a). However, such relationships are not seen in most MORB (Fig. 3a) which are oversaturated with CO_2. This probably results from sluggish CO_2 diffusion in relatively anhydrous basaltic melt that quenches before reaching CO_2 saturation (Dixon et al., 1988).

Saturation pressures calculated from major volatile contents of most Kolbeinsey glasses correspond with confining pressures at the depth of collection (Fig. 3a). This suggests that these glasses had sufficient time for gas saturation to be achieved, and maintained, during eruption (Dixon et al., 1988, Macpherson and Mattey, 1994; Dixon and Stolper, 1995). Some North Kolbeinsey Ridge glasses do not follow this trend due to moderately elevated CO_2 concentrations for their eruption depth. The lower frequency of CO_2 oversaturation in Kolbeinsey glasses, compared to MORB, could reflect (i) longer storage or transport times in the crust, (ii) slower eruption rates, or (iii) more protracted flow histories on the seafloor. Volatile oversaturation factors up to 2.5 on the North Kolbeinsey Ridge (Fig. 3a), suggest magma emplacement and degassing histories beneath the deeper Kolbeinsey Ridge sites becomes similar to those elsewhere on the mid-ocean ridge system.

5.1.2 Evolution of Dissolved Volatiles

The low CO_2 concentrations and variable saturation implies that Kolbeinsey magmas experienced some degassing. Degassing models illustrate that continually exsolving a gas phase from ascending magma results in highly efficient removal of CO_2 with negligible H_2O loss until very low pressures are reached (Fig. 3b). From this, we infer that degassing had a negligible effect on H_2O content of the magmas. Until it becomes saturated, water is incompatible in basaltic melt so fractional crystallisation would lead to higher H_2O contents in the glasses. Similarly, any interaction with the crust would only act to elevate H_2O contents. Therefore, we conclude that the Kolbeinsey Ridge mantle is relatively anhydrous.

The isotopic evolution of magmatic CO_2 during polybaric degassing can be described by two endmember processes (Gerlach and Taylor, 1990). During Batch Equilibrium Degassing (BED) bubbles maintain isotopic equilibrium with the melt from which they exsolve. Fractional Equilibrium Degassing (FED) occurs when bubbles form in isotopic equilibrium with a melt then cease isotopic exchange prior to further degassing. The bubbles formed during either process could subsequently be lost from the magma. As BED and FED progress the $\delta^{13}C$ values of CO_2 in the residual melt will display contrasting evolution (Fig. 4). A variety of approaches have failed to produce a consensus on the most appropriate value for the magnitude of isotopic fractionation between gaseous and dissolve CO_2 ($\Delta_{CO2\text{-}melt}$) in basaltic systems. Values determined experimentally on systems containing CO_2 and basaltic melt, or melt analogues, vary from 2.3‰ to 4.6‰ (Javoy et al., 1978; Mattey, 1991) and empirical data have been modelled using both these extremes (*e.g.* Mattey et al., 1989; Macpherson and Mattey, 1994; Pineau and Javoy, 1994; Cartigny, 2001). An alternative approach is to consider experimental data for only the carbon-bearing parts of the basalt - vapour system. Carbon dissolves in basaltic melt as carbonate ion complexes and exsolves mainly as carbon dioxide (Harris, 1981; Javoy and Pineau, 1991; Fine and Stolper, 1986). The isotopic fractionation between gaseous CO_2 and calcite at magmatic temperatures is approximately 2.3‰ (Scheele and Hoefs, 1992).

CO_2 dissolved in Kolbeinsey Ridge glasses displays a range of $\delta^{13}C$ values that is greater than can be produced by BED from a single starting composition (Fig. 4a and b). The lowest carbon $\delta^{13}C$ values describe a steep array that approximate an FED array with a higher value for $\Delta_{CO2\text{-}melt}$ (Fig. 4a). To test the possibility that degassing occurred with high $\Delta_{CO2\text{-}melt}$ we compare the variation in $\delta^{13}C$ with that of another solubility-controlled parameter, $CO_2/^{40}Ar^*$. First, the concentration and $\delta^{13}C$ value of pre-eruptive CO_2 is determined by assuming that glasses with the highest $\delta^{13}C$ values represent BED and that the array with relatively low $\delta^{13}C$ results from FED (Fig. 4a). (Intermediate values would result from more complex, multi-stage degassing from an initial melt [c.f. Shaw et al., 2004]). Using this approach implies that $\Delta_{CO2\text{-}melt} \sim 4.5‰$ and yields an estimate of the pre-eruptive magma containing 950 ppm CO_2 with $\delta^{13}C$ of -3.5‰. Then, the evolution of $CO_2/^{40}Ar^*$ during fractional degassing is estimated by assuming that the initial value is similar to MORB (21,000; Burnard, 1999) and that the solubility ratio of CO_2 to Ar (S_{CO2}/S_{Ar}) is 4 (Cartingy et al., 2001). The calculated array fails to produce the low $\delta^{13}C$ values required at intermediate $CO_2/^{40}Ar^*$ (dashed line, Fig. 5a). The example in Figure 5a is a "best case scenario" for producing a fit. Alternative estimates of initial $CO_2/^{40}Ar^*$ in MORB (e.g. Cartingy et al., 2001) and S_{CO2}/S_{Ar} (Burnard, 2001) are higher than the value used and would produce greater divergence between the data and the model. Furthermore, most spreading centre magmas probably experience degassing prior to equilibration in the crust (Javoy and Pineau, 1991; Macpherson and Mattey, 1994). Since $S_{CO2}/S_{Ar} > 1$ any prior degassing will increase $CO_2/^{40}Ar^*$ such that residual melt, which provides the starting point for the models in Figures 4 and 5, would also diverge further from the data. Therefore, the coupled CO_2 and Ar data suggest that while employing a $\Delta_{CO2\text{-}melt}$ value of around 4.5‰ can reproduce the CO_2 - $\delta^{13}C$ variation in the Kolbeinsey suite, it cannot produce the relationships observed between CO_2 and noble gases. Since the preferred estimate of $\Delta_{CO2\text{-}melt}$ (2.3‰, see above) produces even less isotopic variation, this modelling also implies that the entire range of $\delta^{13}C$ variation cannot result from degassing alone.

Taking the preferred value for $\Delta_{CO2\text{-}melt}$, we estimate the composition of pre-eruptive CO_2 by once again interpreting the glasses with the highest $\delta^{13}C$ values as products of BED but this time assuming that FED has generated the CO_2 characteristics of the glasses with $\delta^{13}C$ values between -10‰ and

-15‰. This suggests that pre-eruptive melts contained 400 ppm (±100 ppm) CO_2 with a $\delta^{13}C$ value of -6‰ (±1‰; Fig. 4b). Using solubility models and the range of measured H_2O (Dixon and Stolper, 1995), this pre-eruptive dissolved CO_2 concentration would have been in equilibrium with basaltic melt at 0.85kbar, equivalent to 2.7km beneath a ridge that is 1000mbsl or 3.0km beneath a ridge that is 100mbsl. However, this also requires some other process to account for the glasses that have low $\delta^{13}C$ with respect to their CO_2 content. Since the "low-$\delta^{13}C$" array includes glasses from the Tjörnes Fracture Zone, the North Kolbeinsey Ridge and the South Kolbeinsey Ridge it is unlikely that this reflects changes to sources, which tend to vary systematically along the ridge (Mertz et al., 1991; Schilling et al., 1999). Stepped heating has been shown to effectively isolate dissolved CO_2 from secondary contaminant carbon (Macpherson et al., 1999). Therefore, we conclude that the low-$\delta^{13}C$ glasses acquired their distinctive isotopic character when they were still molten.

Two processes other than polybaric degassing can change $\delta^{13}C$ values in volatile-saturated molten basalt. Isobaric degassing will fractionate carbon isotopes (Marty and Zimmerman, 1999) but, since solubility is pressure-dependant, the CO_2 *concentration* will not change unless there is a substantial increase in H_2O (c.f. Fig. 3b). During subsequent (polybaric) degassing the variably crystallised melts would then generate sub-parallel arrays on Figure 4, rather than the diverging arrays observed. Alternatively, isotopically distinct carbon can be added to the melt. Such addition at a single depth would also change $\delta^{13}C$ values but not CO_2 concentrations prior to eruption (c.f. Shaw et al., 2004). Instead, arrays with different slopes (Fig. 4b) require carbon addition during degassing. To simulate this process, we have constructed a model in which small FED increments (of F = 0.0025) are followed by isotopic equilibration with a contaminant (FED-eq). FED was used since longer storage and eruption times are likely to favour interaction between melts and contaminants. The speciation and isotopic composition of carbon in oceanic crust is probably stratified. The top 10s to 100s of metres of the most thoroughly characterised oceanic crust, from hole DSDP Holes 417, 418 (Atlantic Ocean) and 504B (Pacific Ocean), host carbonate with marine $\delta^{13}C$ values (~ 0‰ ± 2‰; Alt et al., 1986; Staudigel et al. 1995). Rocks from greater depths, however, which are likely to represent wall rocks where magma is stored, contain CO_2 and CH_4 with a range of carbon concentrations and isotope ratios. We have used a contaminant possessing 200 ppm CO_2 with $\delta^{13}C$

of –20‰ (Kelley and Früh-Green, 2001). After each degassing increment, 0.25% of the contaminant carbon mixes with the CO_2 remaining dissolved in the melt. Figure 4b illustrates that the low-$\delta^{13}C$ array could result from this type of contamination. The model in Figure 4b is not unique; lower carbon concentrations in the contaminant decrease the change in $\delta^{13}C$ for a given amount of degassing but this can be offset by lower $\delta^{13}C$ in the contaminant. However, the model illustrates that carbon transfer from crust to melt generates CO_2 - $\delta^{13}C$ variations that closely resemble degassing trends with elevated $\Delta_{CO2\text{-}melt}$ (Fig. 4). The FED-eq model is also able to produce low $\delta^{13}C$ relative to $CO_2/^{40}Ar^*$ (Fig. 5a).

Interaction between magmas and Kolbeinsey Ridge crust may also be responsible for the low $^{40}Ar/^{36}Ar$ ratios observed in many of the glasses. There is a strong correlation of $^{40}Ar/^{36}Ar$ with [Ar] and CO_2 suggesting that more degassed glasses acquired Ar with an atmospheric isotope ratio (Fig. 5b and c). This correlation exists for Ar extracted from glass at 1200°C, after heating to 600°C and 800°C. Patterson et al. (1990) suggest that such results are consistent with contamination while the magma was still molten, possibly by seawater or fluids stored in the ocean crust (Kent et al. 1999). However, Ballentine and Barfod (2000) suggest that atmospheric Ar may be incorporated into glass by creation and resealing of fractures, due to vesicle overpressure during recovery from the seafloor or stress during sample handling. Correlations between $^{40}Ar/^{36}Ar$ and gas concentration are most prominent in the North Kolbeinsey Ridge glasses which, in the main, have high $\delta^{13}C$ values. This is more easily reconciled with lowering of $^{40}Ar/^{36}Ar$ by post-eruptive contamination, but also indicates that the low $\delta^{13}C$ carbon signature is independent of atmospheric Ar.

5.1.3 Pre-eruptive Composition and Source of Dissolved Volatiles

H_2O concentrations in Kolbeinsey glasses are comparable with worldwide MORB and there is no evidence to suggest that the Kolbeinsey mantle is more water-rich than the MORB source. The northern Reykjanes Ridge, on the other hand, displays a two-fold increase in water compared to glasses from further south, which Nichols et al. (2002) propose was the result of a direct input from Icelandic mantle. If melt production around Iceland is enhanced by water in the mantle (Asimow and Langmuir, 2003) then Kolbeinsey Ridge and Tjörnes Fracture Zone glasses also should display

elevated H_2O. The low water concentrations north of Iceland suggest that any excess melting responsible for thick crust at Kolbeinsey Ridge (Kodaira et al., 1998) result from a thermal, rather than a chemical, anomaly.

A pre-eruptive CO_2 concentration of ~ 400 ppm is lower than estimates for primitive MORB (Jambon, 1994; Saal et al. 2002; Cartigny et al., 2001) suggesting some degassing may have occurred prior to equilibration at 2.7-3.0km below the seafloor. Degassing of basaltic magma at ocean ridges can be regarded as a two-stage process and the "pre-eruptive" composition identified above could represents the transition between these two stages (Pineau and Javoy, 1983; Macpherson and Mattey, 1994; Cartigney et al., 2001). The highest $\delta^{13}C$ values in Kolbeinsey glasses resemble MORB from many locations (Pineau and Javoy, 1983; Mattey et al., 1984; Exley et al., 1986; Mattey et al., 1989; Pineau and Javoy, 1994) while the pre-eruptive CO_2 concentration and isotope ratio are similar to those determined for other spreading centre glasses (Macpherson and Mattey, 1994; Cartigny et al., 2001; Shaw et al., 2004). If the Kolbeinsey glasses were generated from CO_2–rich primary melts (Kingsley and Schilling, 1995) then they should possess systematically lower $\delta^{13}C$ than other MORB due to having lost a greater proportion of their initial CO_2, unless that CO_2 also possessed higher $\delta^{13}C$ (Exley et al., 1986).

Saal et al. (2002) proposed that CO_2 and niobium have similar distribution coefficients during melting beneath spreading centres and that the relatively constant CO_2/Nb of undegassed MORB provides a means to estimate initial CO_2 content of basaltic melt. Assuming CO_2/Nb of the Kolbeinsey mantle is not significantly different from that at the sites considered by Saal et al. (2002) we can estimate the minimum extent of degassing prior to crustal equilibration at ~3km below the seafloor. Combining their estimate of CO_2/Nb in the upper mantle (239), with Nb concentrations in Kolbeinsey lavas (Devey et al., 1994) suggests that primary magmas contained 380 to 800 ppm CO_2. In this case, Kolbeinsey magmas have experienced 0 to 50% degassing during migration from their sources to sub-ridge magma chambers. With $\Delta_{CO2\text{-}melt}$ = 2.3‰ this would decrease $\delta^{13}C$ values of magmas by up to 1.1‰ before they arrive in magma chambers beneath the ridge. Therefore, the minimum $\delta^{13}C$ value of the mantle beneath the Tjörnes Fracture Zone and Kolbeinsey Ridge lies in the range –5‰ to -6‰.

A minimum estimate for the $^{40}Ar/^{36}Ar$ of the mantle beneath the Kolbeinsey Ridge can be obtained from the highest ratio measured in a glass (5160). This is slightly lower than the highest value measured in Icelandic lavas (6,500; Harrison et al., 1999), although linear extrapolation through the North Kolbeinsey Ridge data to pre-eruptive CO_2 of 400 ppm suggests that $^{40}Ar/^{36}Ar$ may have been as high as 12,500 (Fig. 5c).

5.2 Vesicle Gases

The amount of CO_2 recovered from vesicles can be employed as a proxy for vesicularity since the fraction of CO_2 in vesicles from H_2O-poor lavas exceeds 95% (Harris, 1981; Javoy and Pineau, 1991). At equilibrium, the difference between $\delta^{13}C$ values of dissolved and vesicle CO_2 should equal $\Delta_{CO2\text{-}melt}$, however, Table 1 shows the differences in the Kolbeinsey Ridge data range from –26‰ to +11‰. A gas phase exsolved during BED or FED would possess $\delta^{13}C$ values consistently higher than the pre-eruptive CO_2 (Fig. 4c). The lack of melt – vapour $\delta^{13}C$ equilibrium suggests either (1) that the intermediate heating steps incorporate non-magmatic carbon, or (2) that open system behaviour produced a vesicle cargo that is different from the gas which was in equilibrium with the melts during degassing. We emphasize that extreme care was exercised in screening the samples to minimise alteration or surface deposits, such as carbonate, that might volatilise between 700°C and 900°C during stepped heating. Moreover, samples were thoroughly cleaned in solvents and were combusted at 400°C and 600°C to minimise the effect of any persistent organic contaminants, and a procedural blank correction has been applied. Finally, all but a few analyses were conducted on grain sizes ≥ 2mm which should minimise the effects of organic contamination at intermediate heating (Pineau and Javoy, 1994). Therefore, we interpret the melt – vapour disequilibrium in CO_2 is a product of open system behaviour.

Atmospheric contamination has significantly affected the Ne and Ar isotopic compositions of Kolbeinsey vesicle gas. Most Ne isotope ratios lie within error of air. Those that are significantly different from air tend to have low [Ne] (Fig. 6b) but are most vesicular (Fig. 6d). In contrast, the "air-rich" glasses are those that retain little CO_2. This suggests massive overprinting of Ne by an atmospheric component. In the North Kolbeinsey Ridge $^{40}Ar/^{36}Ar$ decreases with decreasing [Ar]

(Fig. 5b) and the less vesicular samples again tend towards atmospheric compositions (Fig. 6c). This is consistent with addition of a constant amount of atmospheric component to variably degassed glasses (Burnard et al., 1997). However, the remainder of the suite display a wide range in [Ar] with near-atmospheric $^{40}Ar/^{36}Ar$, including some very elevated concentrations (Fig. 5b). Like Ne, this suggests the presence of a large amount of atmospheric Ar in the glasses erupted in the shallowest water.

5.2.1 Evolution of Vesicle Gas

Unlike dissolved components, it is not possible to determine the extent of degassing from solubility data and major volatile concentrations. However, volatile ratios in the gas phase provide information about degassing histories. He is more soluble in basaltic magma than Ar ($S_{He}/S_{Ar} \sim 9.5$; Jambon et al., 1986), therefore residual $^{4}He/^{40}Ar^{*}$ should increase with degassing. Furthermore, low $^{3}He/^{4}He$ ratios are not associated with low [He] (Fig. 6a), suggesting that crustal contamination had a negligible effect on He (Hilton et al., 1993; Hilton et al., 1995; Macpherson et al., 1998; Macpherson et al., 2005). Therefore, in the Kolbeinsey and Tjörnes glasses, $^{4}He/^{40}Ar^{*}$ should reflect only the effects of degassing. For an initial melt $^{4}He/^{40}Ar^{*}$ of 2.5 (Jambon et al., 1985; Marty and Zimmerman, 1999) vapour produced by BED will evolve from 0.26 to 2.5 while the residue will progress from 2.5 to 24 (Fig. 7). Even higher $^{4}He/^{40}Ar^{*}$ can developed through FED (Fig. 7).

Three vesicle splits have $^{4}He/^{40}Ar^{*}$ that lie in the range of BED vapour, the remainder have more elevated values (up to 85) suggesting that they originated in magma that had experienced prior degassing. Most of the North Kolbeinsey Ridge samples possess $^{4}He/^{40}Ar^{*}$ values consistent with moderate amounts of BED. Employing an initial value of 2.5 for $^{4}He/^{40}Ar^{*}$ then we can estimate initial values for $CO_2/^{3}He$ (= 2×10^{9}) and for $CO_2/^{40}Ar^{*}$ (= 40,000) (see Fig. 7), which are similar to or slightly higher than estimates for MORB (Marty and Jambon, 1987; Burnard, 1999; Cartigny et al., 2001). This suggests that, relative to one another, the fluxes of CO_2, He and Ar from the Kolbeinsey mantle are similar to those through Mid-Atlantic Ridge segments which are remote from Iceland. Furthermore, it supports the conclusion that the flux of carbon relative to He in high-

$^{3}He/^{4}He$ magmatism is not dissimilar to that of MORB, *i.e.* $CO_2/^{3}He$ ratios are close to 2×10^{9} (Trull et al., 1993; Marty and Tolstihkin, 1998; Marty and Zimmermann, 1999; Shaw et al., 2004).

While the $^{4}He/^{40}Ar^{*}$ of the remaining glasses can be reconciled with degassing, their $CO_2/^{3}He$ and $CO_2/^{40}Ar^{*}$ ratios are displaced to substantially higher values than predicted by degassing models (Fig. 7). This is also true of the three samples with low $^{4}He/^{40}Ar^{*}$ but is exemplified by the Southern Kolbeinsey Ridge where $CO_2/^{40}Ar^{*}$ and $CO_2/^{3}He$ correlate strongly (Fig. 7c) and increase with $^{4}He/^{40}Ar^{*}$. High CO_2/noble gas ratios can occur in the residues of diffusion controlled degassing (Ozima and Podosek, 1983; Burnard, 2001) but would not produce elevated $^{4}He/^{40}Ar^{*}$ and should be accompanied by higher $\delta^{13}C$ and possibly decreased $^{3}He/^{4}He$ (Burnard et al., 2003), neither of which are observed. A more plausible explanation is that the vesicles are enriched in CO_2. Excess carbon incorporated into magma (e.g. by FED-eq) cannot dissolve in the volatile-saturated melt phase and so will be added instead to the gas phase. There are no direct measurements of $CO_2/^{3}He$ in altered oceanic crust, but old oceanic crust contains less ^{4}He than is predicted from its age and U and Th contents. This suggests that He is lost by degassing and/or diffusion (Staudacher and Allègre, 1988) which would result in high $CO_2/^{3}He$. Shaw et al. (2004) have estimated that in hydrothermally-active areas, crustal $CO_2/^{3}He$ is $\geq 1 \times 10^{11}$. Like He, ^{40}Ar is also less abundant in oceanic crust than projected from the age and K content of DSDP basalts (Staudacher and Allègre, 1988) suggesting that all light noble gases are continually lost from oceanic crust. Thus, contamination is less likely to impact $^{4}He/^{40}Ar^{*}$ due to the crust's paucity in the light noble gases, while CO_2/Ar and CO_2/He will become increasingly susceptible to contamination as degassing reduces gas concentrations in the magma i.e. from Northern to Southern Kolbeinsey Ridge. Carbon isotope ratios of vesicle CO_2 are generally low, consistent with addition of a low-$\delta^{13}C$ contaminant as deduced from the dissolved volatile data. Lower $\delta^{13}C$ values tend to occur in vesicles with higher $CO_2/^{3}He$ although there is not a strong correlation (Fig. 7d) suggesting that there may be some $\delta^{13}C$ heterogeneity in the contaminant (Alt et al. 1986; Staudigel et al., 1995; Kelley and Früh-Green, 2001).

5.2.2 Parental Noble Gas Isotope Ratios

The elevation of $^{3}He/^{4}He$ on Kolbeinsey Ridge, relative to MORB, has been proposed as evidence for northward outflow of mantle from beneath Iceland (Schilling et al., 1999), but the new dataset do not support a gradual decrease of $^{3}He/^{4}He$ from the Tjörnes Fracture Zone to 71°N (Fig. 2f). Instead, the Tjörnes Fracture Zone glasses have slightly higher ratios than Kolbeinsey Ridge, where $^{3}He/^{4}He$ is relatively constant. The lack of systematic variation in $^{3}He/^{4}He$ along Kolbeinsey Ridge is at odds with active dispersal of Icelandic mantle, which is predicted to result in gradual dilution of this component towards the north (Schilling et al., 1999; Breddam et al., 2000). Mertz et al. (1991) proposed that the Tjörnes Fracture Zone may be the surface expression of a barrier to lateral mantle flow immediately north of Iceland, on the basis of inconsistent Sr-Nd-Pb isotope mixing trends between Iceland and Kolbeinsey sources. A barrier is supported by seismic tomography evidence for a significant contrast between mantle to the north and south of the fracture zone (Foulger et al., 2001). However, the elevated $^{3}He/^{4}He$ ratios suggest that Iceland has influenced the Kolbeinsey mantle. This could result from northward, lateral flow of mantle from beneath Iceland at some time in the past when there was no barrier to dispersion. One possibility is that outflow occurred ~ 24 Ma when the Kolbeinsey Ridge formed and the Aegir Ridge became extinct (Vogt et al., 1980; Talwani and Eldholm, 1977; Kodaira et al., 1998). Alternatively, the Kolbeinsey mantle source may have been emplaced in the early Tertiary, at the same time that high-$^{3}He/^{4}He$ magmatism became widespread elsewhere in the North Atlantic (Marty et al., 1998; Graham et al, 1998; Stuart et al., 2003). This conclusion is supported by data for near-axis volcanic rocks from Eggvin Bank where Sr-Nd-Pb isotope ratios are more similar to lavas from southern Iceland than those from north of central Iceland (Mertz et al. 2004). Since there appears to be only limited recent interaction between mantle sources north of Iceland, this resemblance could result from emplacement of a mantle domain during the earliest stages of the North Atlantic large igneous province.

The highest measured $^{20}Ne/^{22}Ne$ ratio lies within error of the Ne-B component ($^{20}Ne/^{22}Ne$ ~ 12.5) that Trieloff et al. (2000) proposed characterises Icelandic mantle but an endmember with solar $^{20}Ne/^{22}Ne$ (13.8) cannot be discounted (Fig. 8). In a $^{20}Ne/^{22}Ne$ versus $^{21}Ne/^{22}Ne$ plot (Fig. 8a), suites of oceanic lavas contaminated by air radiate from the atmospheric composition towards the

primary Ne isotopic composition of any magma series. For example, MORB follow a trend with moderate slope while high-$^{3}He/^{4}He$ Ocean Island Basalts (OIB), such as lavas from Loihi and Iceland, tend to follow steeper trends (Fig. 8a). Whereas the mantle generates negligible amounts of ^{20}Ne and ^{22}Ne (on the scale of Fig. 8a), significant quantities of ^{21}Ne are produced by nuclear reactions during the decay of radioactive U and Th (Kyser and Rison, 1982), thereby effecting measurable changes in $^{21}Ne/^{22}Ne$. Honda et al. (1993) proposed that, since both ^{4}He and ^{21}Ne are ultimately products of the same radioactive decay schemes, then $^{4}He/^{21}Ne^{*}$ (where $^{21}Ne^{*}$ is the amount of nucleogenic ^{21}Ne) should be constant. Thus, for any closed system (i.e. constant $^{3}He/^{22}Ne$) the increase in $^{21}Ne/^{22}Ne$, from an initial solar value, would be proportional to the decrease of $^{3}He/^{4}He$ (Honda et al., 1993). Therefore, the $^{3}He/^{4}He$ of a sample, or suite of samples, can be used to calculate the expected Ne isotope array. Figure 8a shows that the few Kolbeinsey glasses with non-atmospheric Ne lie close to the array predicted for mantle with the mean $^{3}He/^{4}He$ of the Kolbeinsey lavas (11 R_A). This suggests that north of Iceland both $(U+Th)/^{3}He$ and $(U+Th)/^{21}Ne$ are higher than Icelandic mantle, but lower than the source of MORB.

It is possible to assess the fractionation of He from Ne by calculating the $^{3}He/^{22}Ne$ ratio of uncontaminated melts, as described by Moreira et al. (2001):

$$^{3}He/^{22}Ne = [(^{21}Ne/^{22}Ne)_{kol} - (^{21}Ne/^{22}Ne)_{sol}] / [(^{21}Ne/^{4}Ne)^{*} \times \{(^{4}He/^{3}He)_{kol} - (^{4}He/^{3}He)_{sol}\}]$$

where $(^{21}Ne/^{22}Ne)_{kol}$ is the $^{21}Ne/^{22}Ne$ ratio extrapolated to 0% air contamination (= 0.0552) by assuming solar $^{20}Ne/^{22}Ne$ (= 13.8; Benkert et al., 1993), $(^{4}He/^{3}He)_{kol}$ is 65,900 (equivalent to 11.0 R_A), $(^{21}Ne/^{4}Ne)^{*}$ is the mantle production ratio of 4.5×10^{-8}, $(^{21}Ne/^{22}Ne)_{sol}$ is 0.032 and $(^{4}He/^{3}He)_{sol}$ is 5000. This approach gives a $^{3}He/^{22}Ne$ value of 8.5, which is lower than the MORB value of 11 but significantly greater than the value of 4 calculated for magmatism on the Reykjanes peninsula in SW Iceland (Dixon et al., 2000; Moreira et al., 2001). Therefore, Kolbeinsey Ridge represents the transition in light noble gas elemental ratios between those of the Mid-Atlantic Ridge remote from Iceland and those on Iceland itself.

The highest $^{40}Ar/^{36}Ar$ ratio of vesicle gas is slightly less than the maximum value measured in the dissolved component or in the Icelandic Dice lava, although coupled Ne-Ar isotopic variations are

similar to the latter (Fig. 8b). Harrison et al. (1999) suggest that the Dice lava was derived from a source with $^{40}Ar/^{36}Ar$ ~7,500, which is lower than the value extrapolated from dissolved Ar and CO_2 (Fig. 5c). However, both values are substantially lower than estimates for the MORB source (~40,000, Burnard et al. 1997).

6. CONCLUSIONS

1. Water contents of Kolbeinsey Ridge and Tjörnes Fracture Zone glasses are similar to N-MORB. There is no evidence that the water concentrations of Kolbeinsey Ridge magmas or their mantle sources increase towards Iceland.

2. Degassing has strongly affected the CO_2 and He contents of Kolbeinsey Ridge and Tjörnes Fracture Zone glasses but cannot be responsible for the range of $\delta^{13}C$ values or the relationship of CO_2 to noble gases. Carbon addition from altered oceanic crust has lowered the $\delta^{13}C$ values of CO_2 dissolved in glasses and contained in vesicles and elevated the CO_2/Ar and CO_2/He ratios of vesicle gas.

3. Pre-eruptive $\delta^{13}C$ values and CO_2/Ar and CO_2/He ratios of Kolbeinsey Ridge magmas cannot be distinguished from MORB. If CO_2 contents in the Kolbeinsey mantle are similar to MORB-source mantle, then light noble gases contents also resemble MORB. Alternatively, if the mantle north of Iceland contains more CO_2 than the MORB source then (i) the light noble gases are enriched by a similar factor, and (ii) its $\delta^{13}C$ value is higher than MORB.

4. $^{3}He/^{4}He$, $^{40}Ar/^{36}Ar$ and fractionation of He from Ne in the Kolbeinsey Ridge glasses are transitional between MORB and Icelandic magmatism. The variation of $^{40}Ar/^{36}Ar$ with $^{20}Ne/^{22}Ne$ is similar to Icelandic magmas.

5. Kolbeinsey Ridge glasses possess higher $^{3}He/^{4}He$ than MORB, suggesting involvement of Icelandic mantle in the past, but the lack of $^{3}He/^{4}He$ variation along the ridge is not consistent with active mantle outflow from beneath Iceland at the present time. More elevated $^{3}He/^{4}He$ values within the Tjörnes Fracture Zone suggest that this marks the northern limit of Icelandic mantle outflow at shallow levels.

ACKNOWLEDGEMENTS

This research was supported by start-up funds to DRH from Scripps Institution of Oceanography, and grants from NSF (EAR-9614347) to DRH and from NERC (NER/M/S/2001/00099) to CGM. Kathy Ponganis and Thomas Graf provided CGM with instruction on operating the VG5400. Martin Wahlen kindly allowed us access to his laboratory to conduct carbon isotope measurements, with which Bruce Deck assisted. David Mattey is thanked for access to use his laboratory where Alison Shaw measured water abundances. Discussions with many colleagues have helped shaped our thinking. Highly constructive comments and suggestions by Peter Burnard and Jacqueline Dixon and the comments of an anonymous reviewer improved this submission. We thank Bernard Marty for editorial handling and valuable comments.

REFERENCES

Alt J. C., Muehlenbachs K. and Honnorez J. (1986) An oxygen isotopic profile through the upper kilometre of the oceanic crust, DSDP Hole 504B. *Earth Planet. Sci. Lett.* **80**, 217-229.

Applegate B. (1997) Modes of axial reorganization on a slow-spreading ridge: The structural evolution of Kolbeinsey Ridge since 10Ma. *Geology* **25**, 431-434.

Asimow P. D. and Langmuir C. H. (2003) The importance of water to oceanic mantle melting regimes. *Nature* **421**, 815-820.

Ballentine C. J. and Barfod D. N. (2000) The origin of air-like noble gases in MORB and OIB. *Earth Planet. Sci. Lett*. **180**, 39-48.

Benkert J.-P., Baur H., Signer P. and Wieler R. (1993) He, Ne and Ar from the solar wind and solar energetic particles in lunar ilmenites and pyroxenes. *J. Geophys. Res*. **98**, 13147-13162.

Botz R., Winckler G., Bayer R., Schmitt M., Schmidt M., Garbe-Schobnerg D., Stoffers P. and Kristjansson J.K. (1999) Origin of trace gases in submarine hydrothermal vents of the Kolbeinsey Ridge, north Iceland. *Earth Planet. Sci. Lett.* **171**, 83-93.

Breddam K., Kurz M. D. and Storey M. (2000) Mapping out the conduit of the Iceland mantle plume with helium isotopes. *Earth Planet. Sci. Lett.* **176**, 45-55.

Burnard P. (1999) The bubble-by-bubble volatile evolution of two mid-ocean ridge basalts. *Earth Planet. Sci. Lett.* **174**, 199-211.

Burnard P. (2001) Correction for volatile fractionation in ascending magmas: noble gas abundance in primary mantle melts. *Geochim. Cosmochim. Acta* **65**, 2605-2614.

Burnard P. G., Stuart F. M. and Turner G. (1994) Air contamination of basaltic magmas: Implications for high $^{3}He/^{4}He$ mantle Ar isotopic composition. *J. Geophys. Res*. **99**, 17709-17715.

Burnard P., Graham D. and Turner G. (1997) Vesicle-specific noble gas analyses of "popping rock"; implications for primordial noble gasses in Earth. *Science* **276**, 568-571.

Burnard P., Harrison D., Turner G. and Nesbitt R. (2003) Degassing and contamination of noble gases in Mid-Atlantic Ridge basalts. *Geochem. Geophys. Geosys*. **4**, 2002GC000326.

Burnard P., Graham D., Farley K. (2004) Fractionation of noble gases (He, Ar) during MORB mantle melting: a case study on the Southeast Indian Ridge. *Earth Planet. Sci. Lett*. **227**, 457-472.

Carroll M. R. and Webster J. D. (1994) Solubilities of sulphur, noble gases, nitrogen, chlorine and fluorine in magmas. In: *Volatiles in Magmas*. (eds. M.R. Carroll and J.R. Holloway) Reviews in Mineralogy **30**, 231-279.

Cartigny P., Jendrzejewski N., Pineau F., Petit E. and Javoy M. (2001) Volatile (C, N, Ar) variability in MORB and the respective roles of mantle source heterogeneity and degassing: the case of the Southwest Indian Ridge. *Earth Planet. Sci. Lett*. **194**, 241-257.

Condomines M., Grönvold K., Hooker P. J., Meuhlenbachs K., O'Nions R. K., Oskarsson N. and Oxburgh E.R. (1983) Helium, oxygen and strontium isotopic relationships in Icelandic volcanics. *Earth Planet. Sci. Lett*. **66**, 125-136.

Craig H., Marti K. and Wiens R. (1993) A static mass spectrometer with triple collection for nitrogen and neon isotopes. S.I.O. Reference Series Scripps Inst. Oceanography #93-11, pp 20.

Des Marais D. (1986) Carbon abundance measurement in oceanic basalts: the need for a consensus. *Earth Planet. Sci. Lett*. **79**, 21-26.

Devey C. W., Garbeschonberg C. D., Stoffers P., Chauvel C. and Mertz D. F. (1994) Geochemical effects of dynamic melting beneath ridges – reconciling major and trace element variations in Kolbeinsey (and global) mid-ocean ridge basalt. *J. Geophys. Res*. **99**, 9077-9095.

Dixon J. E. and Stolper E. M. (1995) An experimental study of water and carbon dioxide solubilities in mid-ocean ridge basaltic liquids. Part II: Applications to degassing. *J. Petrol*. **36**, 33-1646.

Dixon J. E., Stolper E. and Delaney J. R. (1988) Infrared spectroscopic measurements of CO_2 and H_2O in Juan de Fuca basaltic glasses. *Earth Planet. Sci. Lett*. **90**, 87-104.

Dixon J. E., Clauge D. A. and Stolper E. M. (1991) Degassing history of water, sulfur and carbon in submarine lavas from Kilauea volcano, Hawaii. *J. Geol*. **99**, 371-394.

Dixon E. T., Honda M., McDougall I., Campbell I. H. and Sigurdsson I. (2000) Preservation of near-solar neon isotopic ratios in Icelandic basalts. *Earth Planet. Sci. Lett*. **180**, 309-324.

Exley R. A., Mattey D. P., Clauge D. A. and Pillinger C. P. (1986) Carbon isotope systematics of a mantle hotspot: a comparison of Loihi seamount and MORB glasses. *Earth Planet. Sci. Lett*. **78**, 189-199.

Fine G. and Stolper E. (1986) Dissolved carbon dioxide in basaltic glasses: concentration and speciation. *Earth Planet. Sci. Lett*. **76**, 263-278.

Foulger G. R., Pritchard M. J., Julian B. R., Evans J. R., Allen R. M., Nolet G., Morgan W. J., Bergsson B. H., Erlendsson P., Jakobsdottir S., Ragnarsson S., Stefansson R., Vogfjord K. (2001) Seismic tomography shows that upwelling beneath Iceland is confined to the upper mantle. *Geophys. J. Int*. **146**, 504-530.

Gerlach T. M. and Taylor B. E. (1990) Carbon isotope constraints on degassing of carbon dioxide from Kilauea volcano. *Geochim. Cosmochim. Acta* **54**, 2051-2058.

Graham D. W. (2002) Noble gas isotope geochemistry of mid-ocean ridge and ocean island basalts: Characterization of mantle source reservoirs. In: *Noble gases in Geochemistry and Cosmochemistry* (eds. D.P. Porcelli, C.J. Ballentine and R. Wieler). Reviews in Mineralogy and Geochemistry **47**, 247-317.

Graham D. W., Larsen L. M., Hanan B. B., Storey M., Pedersen A. K. and Lupton J. E. (1998) Helium isotope composition of the early Iceland mantle plume inferred from Tertiary picrites of West Greenland. *Earth Planet. Sci. Lett*. **160**, 241-255.

Gudmundsson A. (1995) Ocean-ridge discontinuities in Iceland. *J. Geol. Soc*. **152**, 1011-1015.

Harris D. M. (1981) The concentration of CO_2 in submarine tholeiitic basalts. *J. Geol.* **89**, 689-701.

Harrison D., Burnard P. and Turner G. (1999) Noble gas behaviour and composition in the mantle: constraints from the Iceland plume. *Earth Planet. Sci. Lett*. **171**, 199-207.

Hilton D.R., Grönvold K., O'Nions R.K. and Oxburgh, E.R. (1990) Regional distribution of ^{3}He anomalies in the Icelandic crust. *Chem. Geol.* **88**, 53-67.

Hilton D. R., Barling J. and Wheller G. E. (1995) Effects of shallow-level contamination on the helium isotope systematics of ocean-island lavas. *Nature* **373**, 330-333.

Hilton D. R., McMurtry G. M. and Goff F. (1998) Large variations in vent fluid $CO_2/^3$He ratios signal rapid changes in magma chemistry at Loihi seamount, Hawaii. *Nature* **396**, 359-362.

Hilton D. R., Hammerschmidt K., Loock G. and Friedrichsen H. (1993) Helium and argon isotope systematics of the central Lau Basin and Valu Fa Ridge: Evidence of crust/mantle interactions in a backarc basin. *Geochim. Cosmochim. Acta* **57**, 2819-2841.

Hilton D. R., Grönvold K., Macpherson C. G. and Castillo P. R. (1999) Extreme ^{3}He/^{4}He ratios in northwest Iceland: constraining the common component in mantle plumes. *Earth Planet. Sci. Lett*. **173**, 53-60.

Hilton D. R., Thirlwall M. F., Taylor R. N., Murton B. J. and Nichols A. J. (2000) Controls on magmatic degassing along the Reykjanes Ridge with implications for the helium paradox. *Earth Planet. Sci. Lett.* **183**, 43-50.

Hiyagon H., Ozima M., Marty B., Zashu S. and Sakai H. (1992) Noble gases in submarine glasses from mid-ocean ridges and Loihi seamount: Constraints on the early degassing history of the Earth. *Geochim. Cosmochim. Acta* **56**, 1301-1316.

Honda M., McDougall I. and Patterson D. (1993) Solar noble gases in the Earth: The systematics of helium-neon isotopes in mantle derived samples. *Lithos* **30**, 257-265.

Jambon A. (1994) Earth degassing and large-scale geochemical cycling of volatile elements. In: *Volatiles in Magmas* (eds. M.J. Carroll and J.R. Holloway). Reviews in Mineralogy **30**, Mineralogical Society of America, 479-517.

Jambon A., Weber H. W. and Bergmann F. (1985) Helium and argon from an Atlantic MORB glass: concentration, distribution and isotopic composition. *Earth Planet. Sci. Lett.* **73**, 255-267.

Jambon A., Weber H. W. and Braun O. (1986) Solubility of He, Ne, Ar, Kr and Xe in a basalt melt in the range 1250-1600°C. Geochemical Implications. *Geochim. Cosmochim. Acta* **50**, 401-408.

Javoy M. and Pineau F. (1991) The volatiles record of a "popping" rock from the Mid-Atlantic Ridge at 14°N: chemical and isotopic composition of gas trapped in the vesicles. *Earth Planet. Sci. Lett.* **107**, 598-611.

Javoy M., Pineau F. and Iiyama I. (1978) Experimental determination of the isotopic fractionation between gaseous CO_2 and carbon dioxide dissolved in tholeiitic magma. *Contrib. Mineral. Petrol.* **67**, 35-39.

Kelley D. S. and Früh-Green G. L. (2001) Volatile lines of descent in submarine plutonic environments: Insights from stable isotope and fluid-inclusion analyses. *Geochim. et Cosmochim. Acta* **65**, 3325-3346.

Kent A. J. R., Norman M. D., Hutcheon I. D. and Stolper E. M. (1999) Assimilation of seawater-derived components in an oceanic volcano: evidence from matrix glass and glass inclusions from Loihi seamount, Hawaii. *Chem. Geol.* **156**, 299-319.

Kingsley R. H. and Schilling J.-G. (1995) Carbon in Mid-Atlantic Ridge basalt glasses from 28°N to 63°N: Evidence for a carbon-enriched Azores mantle plume. *Earth Planet. Sci. Lett.* **129**, 31-53.

Kodaira S., Mjelde R., Gunnarsson K., Shiobara H. and Shimamura H. (1998) Evolution of oceanic crust on the Kolbeinsey Ridge, north of Iceland over the past 22 Myr. *Terra Nova* **10**, 27-31.

Kurz M. D., Jenkins W. J. and Hart S. R. (1985) Helium isotopic systematics of oceanic islands and mantle heterogeneity. *Nature* **297**, 43-47.

Kurz M. D., Jenkins W. J., Schilling J. G. and Hart S. R. (1982) Helium isotopic variations in the mantle beneath the central North Atlantic Ocean. *Earth Planet. Sci. Lett*. **58**, 1-14.

Kyser K. T. and Rison W. (1982) Systematics of rare gas isotopes in basaltic lavas and ultramafic xenoliths. *J. Geophys. Res*. **87**, 6511-5630.

Macpherson C. G. and Mattey D. P. (1994) Carbon isotope variations of CO_2 in Lau Basin basalts and ferrobasalts. *Earth Planet. Sci. Lett*. **121**, 263-276.

Macpherson C. G., Hilton D. R., Newman S. and Mattey, D. P. (1999) CO_2, $^{13}C/^{12}C$ and H_2O variability in natural basaltic glasses: A study comparing stepped heating and FTIR spectroscopic techniques. *Geochim. Cosmochim. Acta* **63**, 1805-1813.

Macpherson C. G., Hilton D. R., Sinton J. M., Poreda R. J. and Craig H. (1998) High $^3He/^4He$ ratios in the Manus backarc basin: Implications for mantle mixing and the origin of plumes in the western Pacific Ocean. *Geology* **26**, 1007-1010.

Macpherson C. G., Hilton D. R., Day J. M. D., Lowry D., Grönvold K. (2005) High-$^3He/^4He$, depleted mantle and low-$d^{18}O$, recycled oceanic lithosphere in the source of central Iceland magmatism. *Earth Planet. Sci. Lett*. **233**, 411-427.

Mamyrin B. A., Tolstikhin I. N., Anufriyev G. S. and Kamenskiy I. L. (1972) Isotopic composition of helium in Icelandic hot springs. *Geokhimiya* **11**, 1396-1397.

Marty B. and Jambon A. (1987) $C/^3He$ in volatile fluxes from the solid Earth: implications for carbon geodynamics. *Earth Planet. Sci. Lett*. **83**, 16-26.

Marty B. and Tolstikhin I. N. (1998) CO_2 fluxes from mid-ocean ridges, arc and plumes. *Chem. Geol*. **145**, 233-248.

Marty B. and Zimmermann L. (1999) Volatiles (He, C, N, Ar) in mid-ocean ridge basalts: Assessment of shallow-level fractionation and characterization of source composition. *Geochim. Cosmochim. Acta* **63**, 3619-3633.

Marty B., Upton B. G. and Ellam R. M. (1998) Helium isotopes in early Tertiary basalts, northeast Greenland: Evidence for 58Ma plume activity in the North Atlantic - Iceland volcanic province. *Geology* **26**, 407-410.

Mattey D. P. (1991) Carbon dioxide solubility and carbon isotope fractionation in basaltic melt. *Geochim. Cosmochim. Acta* **55**, 3467-3473.

Mattey D. P., Exley R. A. and Pillinger C. T. (1989) Isotopic composition of CO_2 and dissolved carbon in basalt glass. *Geochim. Cosmochim. Acta* **53**, 2377-2386.

Mattey D. P., Carr R. H., Wright I. P. and Pillinger C. T. (1984) Carbon isotopes in submarine basalts. *Earth Planet. Sci. Lett*. **70**, 196-206.

Mertz D. F. and Haase K. M. (1997) The radiogenic isotope composition of the high-latitude North Atlantic mantle. *Geology* **25**, 411-414.

Mertz D. F., Devey C. W., Todt W., Stoffers P. and Hofmann, A. W. (1991) Sr-Nd-Pb isotope evidence against plume-asthenosphere mixing north of Iceland. *Earth Planet. Sci. Lett*. **107**, 243-255.

Mertz D.F., Sharp W.D. and Haase K.M. (2004) Volcanism on the Eggvin Bank (Central Norwegian-Greenland Sea, latitude ~ 71°N): age, source, and relationship to the Iceland and putative Jan Mayen plumes. *J. Geodynamics* **38**, 57-83.

Michael P. (1995) Regionally distinctive sources of depleted MORB: Evidence from trace elements and H_2O. *Earth Planet. Sci. Lett*. **131**, 301-320.

Michael P. and Cornell W. C. (1998) Influence of spreading rate and magma supply on crystallization and assimilation beneath mid-ocean ridges: Evidence from chlorine and major element chemistry of mid-ocean ridge basalts. *J. Geophys. Res.* **103**, 18325-18356.

Moreira M., Kunz J. and Allègre C. (1998) Rare gas systematics in popping rock: isotopic and elemental compositions in the upper mantle. *Science* **279**, 1178-1181.

Moreira M., Breddam K., Curtice J. and Kurz M. D. (2001) Solar neon in the Icelandic mantle: new evidence for an undegassed lower mantle. *Earth Planet Sci. Lett*. **185**, 15-23.

Newman S. and Lowentern J. B. (2002) VOLATILECALC: a silicate melt-H_2O-CO_2 solution model written in Visual Basin for excel. *Computers and Geosciences* **28**, 597-604.

Nichols A. R. L., Carroll M. R. and Höskuldsson Á. (2002) Is the Iceland hotspot also wet? Evidence from the water content of undegassed submarine and subglacial pillow basalts. *Earth Planet. Sci. Lett*. **202**, 77-87.

Niedermann S., Graf T. and Marti K. (1993) Mass spectrometric identification of cosmic-ray-produced neon in terrestrial rocks with multiple neon components. *Earth Planet. Sci. Lett*. **118**, 65-73.

Ozima M. and Podosek, F. A. (1983) *Noble Gas Geochemistry*. Cambridge University Press.

Patterson D. B., Honda M. and McDougall I. (1990) Atmospheric contamination: A possible source for heavy noble gases in basalts from Loihi Seamount, Hawaii. *Geophys. Res. Lett*. **17**, 705-708.

Pineau F. and Javoy M. (1983) Carbon isotopes and concentrations in mid-ocean ridge basalts. *Earth Planet. Sci. Lett*. **62**, 239-257.

Pineau F. and Javoy M. (1994) Strong degassing at ridge crests: the behaviour of dissolved carbon and water in basalt glasses at 14°N, Mid-Atlantic Ridge. *Earth Planet. Sci. Lett*. **123**, 179-198.

Poreda R. and di Brozolo F. R. (1984) Neon isotope variations in Mid-Atlantic Ridge basalts. *Earth Planet. Sci. Lett*. **69**, 277-289.

Poreda R., Schilling J.-G. and Craig H. (1986) Helium and hydrogen isotopes in ocean-ridge basalts north and south of Iceland. *Earth Planet. Sci. Lett*. **78**, 1-17.

Poreda R. J., Craig H., Arnórsson S. and Whelan J. A. (1992) Helium isotopes in Icelandic geothermal systems: I. ^{3}He, gas chemistry and ^{13}C relations. *Geochim. Cosmochim. Acta* **56**, 4221-4228.

Saal A. E., Hauri E. H., Langmuir C. H. and Perfit M. R. (2002) Vapour undersaturation in primitive mid-ocean-ridge basalt and the volatile content of the Earth's upper mantle. *Nature* **419**, 451-455.

Sano Y., Urabe A., Wakita H., Chiba H., Sakai H. (1985) Chemical and isotopic compositions of gases in geothermal fluids in Iceland. *Geochem. J*. **19**, 135-148.

Sarda P. and Graham D. (1990) Mid-ocean ridge popping rocks: implications for degassing at ridge crests. *Earth Planet. Sci. Lett*. **97**, 268-289.

Sarda P., Staudacher T. and Allègre C. J. (1985) ^{40}Ar/^{36}Ar in MORB glasses: constraints on atmosphere and mantle evolution. *Earth Planet. Sci. Lett*. **72**, 357-375.

Sarda P., Staudacher T. and Allègre C. J. (1988) Neon isotopes in submarine basalts. *Earth Planet. Sci. Lett*. **91**, 73-88.

Scheele N. and Hoefs J. (1992) Carbon isotope fractionation between calcite, graphite and CO_2: an experimental study. *Contrib. Mineral. Petrol.* **112**, 35-45.

Schilling J.-G., Kingsley R., Fontignie D., Poreda R. and Xue S. (1999) Dispersion of the Jan Mayen and Iceland mantle plumes in the Arctic: A He-Pb-Nd-Sr isotope tracer study of basalts from the Kolbeinsey, Mohns, and Knipovich Ridges. *J. Geophys. Res.* **104**, 10543-10569.

Shaw A. M., Hilton D. R., Macpherson C. G. and Sinton J. M. (2004) The CO_2-He-Ar-H_2O systematics of the Manus back-arc basin: Resolving source composition from degassing and contamination effects. *Geochim. Cosmochim. Acta* **68**, 1837-1856.

Staudacher T. and Allègre C. J. (1988) Recycling of oceanic crust and sediments: the noble gas subduction barrier. *Earth Planet. Sci. Lett*. **89**, 173-183.

Staudigel H., Davies G. R., Hart S. R., Marchant K. M. and Smith M. (1995) Large scale isotopic Sr, Nd and O isotopic anatomy of altered oceanic crust: DSDP/ODP sites 417/418. *Earth Planet. Sci. Lett*. **130**, 169-185.

Stuart F., Turner G., and Taylor R. (1994) He-Ar isotope systematics of fluid inclusions: resolving mantle and crustal contributions to hydrothermal fluids. In: *Noble Gas Geochemistry and Cosmochemistry* (ed. J. Matsuda), Terra Science, Tokyo 261-277.

Stuart F. M., Lass-Evans S., Fitton J. G. and Ellam R. M. (2003) High $^{3}He/^{4}He$ ratios in pictritic basalts from Baffin Island and the role of a mixed reservoir in mantle plumes. *Nature* **424**, 57-59.

Talwani M. and Eldholm O. (1977) Evolution of Norwegian – Greenland Sea: Recent results and outstanding problems. *Bull. Geol. Soc. Am.* **88**, 969-999.

Thirlwall M. F., Gee M. A. M., Taylor R. N. and Murton B. J. (2004) Mantle components in Iceland and adjacent ridges investigated using double-spike Pb isotope ratios. *Geochim. Cosmochim. Acta* **68**, 361-386.

Trieloff M., Kunz J., Clague D. A., Harrison D. and Allègre C. J. (2000) The nature of pristine noble gases in mantle plumes. *Science* **288**, 1036-1038.

Trull T., Nadeau S., Pineau F., Polvé M. and Javoy M. (1993) C-He systematics in hotspot xenoliths: Implications for mantle carbon contents and carbon recycling. *Earth Planet. Sci. Lett*. **118**, 43-64.

Vogt P. R. (1983) The Iceland mantle plume: Status of hypothesis after a decade of new work. In: *Structure and Development of the Greenland – Scotland Ridge* (ed. M.H.P. Bott) Plenum, New York, 191-213.

Vogt P. R., Johnson G. L. and Kristjansson L. (1980) Morphology and magnetic anomalies north of Iceland. *J. Geophys.* **47**, 67-80.

FIGURE CAPTIONS

Figure 1. (a) Map of the Mid-Atlantic Ridge between Iceland and the Jan Mayen Fracture Zone with locations of dredge sites indicated. Depths are indicated in metres. (b) Mid-Atlantic Ridge north and south of Iceland. TFZ is the Tjörnes Fracture Zone.

Figure 2. Latitudinal variations in (a) collection depth, (b) H_2O content, (c) CO_2 content, (d) $\delta^{13}C$, (e) He content, (f) $^{3}He/^{4}He$, (g) Ne content, (h) $^{20}Ne/^{22}Ne$, (i) Ar content, and (j) $^{40}Ar/^{36}Ar$ of glasses from the Tjörnes Fracture Zone, Kolbeinsey Ridge and Mohns Ridge. Vertical dashed lines give the locations of the Jan Mayen Fracture Zone, the Spar Offset and the northern limit of the Tjörnes Fracture Zone. The error bar in (b) illustrates the uncertainty on H_2O concentration data. Black circles in (e) and (f) are from Schilling et al. (1999 and references therein) and in (g) and (h) are data from Poreda and di Brozolo (1984). Horizontal lines in (h) and (j) give the isotopic ratio of atmosphere.

Figure 3. (a) Comparison between the pressure at which the dissolved CO_2 and H_2O of Kolbeinsey Ridge and Tjörnes Fracture Zone glasses would be saturated and eruption pressure. Saturation pressures were calculated using VOLATILECALC 1.1 (Newman and Lowenstern, 2002), while collection depths are used to approximate eruption pressure. Data for the submarine portion of Kilauea (Dixon et al. 1991), for MORB from the Juan de Fuca Ridge (Dixon et al. 1988), and a 1:1 correspondence line (dashed) are shown for comparison. (b) Concentration of dissolved CO_2 versus H_2O in Kolbeinsey Ridge and Tjörnes Fracture Zone glasses. Solid, sub-horizontal curves are isobars calculated for basalt containing 49 wt.% SiO_2 at 1200ºC using VOLATILECALC 1.1 (Newman and Lowenstern, 2002). Sub-vertical curves are degassing paths modelled using VOLATILECALC 1.1 for degassing of melts initially containing 500 ppm CO_2 and water contents of 0.2 and 0.25 wt.%.

Figure 4. (a) $\delta^{13}C$ versus concentration of dissolved CO_2 for Kolbeinsey Ridge and Tjörnes Fracture Zone glasses. Curves illustrate assumed BED (batch equilibrium degassing; solid curve) and FED (fractional equilibrium degassing; dashed, black curve) trends with $\Delta_{CO2\text{-}melt}$ of 4.5‰ used to estimate that the initial melt contained ~950 ppm CO_2 with $\delta^{13}C$ of –3.5‰ (Macpherson and Mattey, 1994). After ~95% degassing by BED some magmas begin to degas by FED (dashed grey curve). (b) Similar modelling for BED and FED with $\Delta_{CO2\text{-}melt}$ of 2.3‰ yields an estimated initial magma containing 400 ppm CO_2 with $\delta^{13}C$ of –6.0‰. Vertical grey lines indicate F = 0.5 and 0.05. The black, dash-dot curve illustrates isotopic exchange with low-$\delta^{13}C$ material during fractional degassing (FED-eq). The contaminant contains 200 ppm CO_2 with $\delta^{13}C$ of –20‰ and exchanges carbon with the melt during degassing (see text). (c) $\delta^{13}C$ versus abundance of CO_2 vesicle. BED evolution of residual magma is illustrated along with models for the development of gas released from the magma by BED and FED. Tick marks give the fraction of CO_2 remaining dissolved in the melt.

Figure 5. Variations in concentrations and isotopic ratios of CO_2 and Ar in the Kolbeinsey Ridge and Tjörnes Fracture Zone glasses. Open symbols are gas collected at 800°C and grey symbols are gas collected at 1200°C. (a) $CO_2/^{40}Ar^*$ versus $\delta^{13}C$. Black, dashed curve shows FED with $\Delta_{CO2\text{-}melt}$ of 4.5‰, initial $\delta^{13}C$ of -3.5‰ (see Fig. 4a), initial $CO_2/^{40}Ar^*$ of 21,000 (Burnard, 1999) and

S_{CO_2}/S_{Ar} of 4 (Cartigney et al., 2001). Evolution of $CO_2/^{40}Ar^*$ was calculated using a simple Rayleigh fractionation model for two elements *i* and *j* with solubilities S*i* and S*j*, respectively; where $(i/j) = (i/j)_{initial} \times F^{[1-(Si/Sj)]}$. Solid curve shows BED with $\Delta_{CO2\text{-}melt}$ of 2.3‰ and initial $CO_2/^{40}Ar^*$ of 40,000 estimated from vesicle systematics. Black, dash-dot curve illustrates FED-eq with a low-$\delta^{13}C$ component, $\Delta_{CO2\text{-}melt}$ of 2.3‰ and initial $\delta^{13}C$ as calculated in Fig. 4b. Tick marks show the fraction of residual dissolved CO_2. (b) $^{40}Ar/^{36}Ar$ versus [Ar]. Ar-rich rocks possess Ar isotope ratios that range from atmospheric to >5,000, while Ar-poor rocks have strongly atmospheric isotope ratios. (c) $^{40}Ar/^{36}Ar$ versus CO_2.

Figure 6. (a) $^3He/^4He$ versus [He] for vesicle gas from Kolbeinsey Ridge and Tjörnes Fracture Zone glasses. Data from Poreda et al. (1986) are shown for comparison. There are no significant variations amongst the data from Kolbeinsey Ridge. (b) $^{20}Ne/^{22}Ne$ versus [Ne] for vesicle gas. Data from Poreda and di Brozolo (1984) are shown for comparison. The most Ne-rich glasses are indistinguishable from atmosphere. Plots of (c) $^{40}Ar/^{36}Ar$ and (d) $^{20}Ne/^{22}Ne$ versus abundance of vesicle CO_2 in Kolbeinsey Ridge and Tjörnes Fracture Zone glasses show that mantle isotopic ratios for Ar and Ne are preserved in rocks containing the most vesicles (*i.e.* most CO_2).

Figure 7. (a) $^4He/^{40}Ar^*$ versus $CO_2/^{40}Ar^*$, (b) $^4He/^{40}Ar^*$ versus $CO_2/^3He$, and (c) $CO_2/^{40}Ar^*$ versus $CO_2/^3He$ in vesicle gas from Kolbeinsey Ridge and Tjörnes Fracture Zone glasses. Model degassing curves are shown for the gas phase (black, solid curve) and residual melt (black, dashed curve) during BED and for a melt undergoing FED (solid grey curve). The initial melt has $CO_2/^3He$ of 2.2×10^9, $CO_2/^{40}Ar^*$ of 40,000 and $^4He/^{40}Ar^*$ of 2.5. Solubilities are as used in modelling the dissolved species, with $S_{He}/S_{CO_2} = 2.4$ (Hilton et al., 1998). Models were calculated using the method of Jambon et al. (1986). Ticks on curves represent vesicularities and are marked at values of 0.0005, 0.001, 0.005, 0.01 and 0.05 unless labelled otherwise. The composition of initial vapour (iv) and final residual melt (frm) produced by BED are indicated by small grey dots, and an arrow shows the sense of degassing for the FED model. (d) $\delta^{13}C$ versus $CO_2/^3He$ in vesicle gas. FED of a melt with $CO_2/^3He$ of 2.2×10^9 and $\delta^{13}C$ of –6.2‰ are shown for $\Delta_{CO2\text{-}melt}$ values of 2.3‰ (solid line) and 4.5‰ (dashed line). Vertical grey lines illustrate how F varies in both models.

Figure 8. (a) $^{20}Ne/^{22}Ne$ versus $^{21}Ne/^{22}Ne$ in vesicle gas from Kolbeinsey Ridge glasses. For clarity, the plot illustrates only those samples from the Kolbeinsey Ridge in which Ne is significantly different from air (at the 1σ level). The composition of air, a MORB curve (Sarda et al., 1988), popping rock 2πD43 (Moreira et al., 1998), and Icelandic lava Dice (Trieloff et al., 2000) are shown for comparison. There is a good agreement between the Kolbeinsey data and the trend calculated for mantle with the average Kolbeinsey $^{3}He/^{4}He$ (grey line; Honda et al., 1993). (b) $^{40}Ar/^{36}Ar$ versus $^{20}Ne/^{22}Ne$ in vesicle gas from Kolbeinsey Ridge and Tjörnes Fracture Zone glasses. Data for popping rock 2πD43 (Moreira et al., 1998) and the Icelandic lava Dice (Trieloff et al., 2000) are shown for comparison.

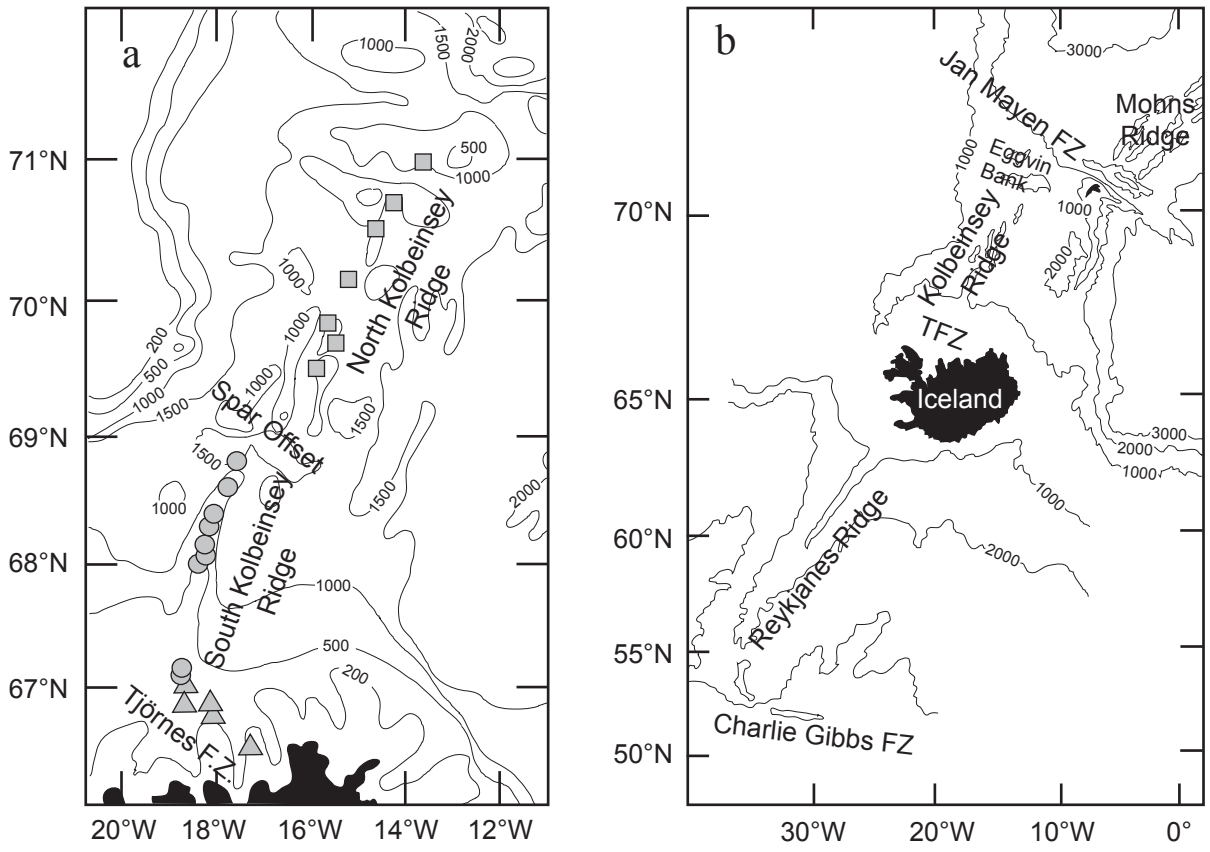
a
b
71°N
70°N
69°N
68°N
67°N
20°W
18°W
16°W
14°W
12°W
North Kolbeinsey Ridge
Spar Offset
South Kolbeinsey Ridge
Tjörnes F.Z.
Jan Mayen FZ
Mohns Ridge
Eggvin Bank
Kolbeinsey Ridge
TFZ
Iceland
Reykjanes Ridge
Charlie Gibbs FZ
65°N
60°N
55°N
50°N
30°W
20°W
10°W
0°

Figure 1

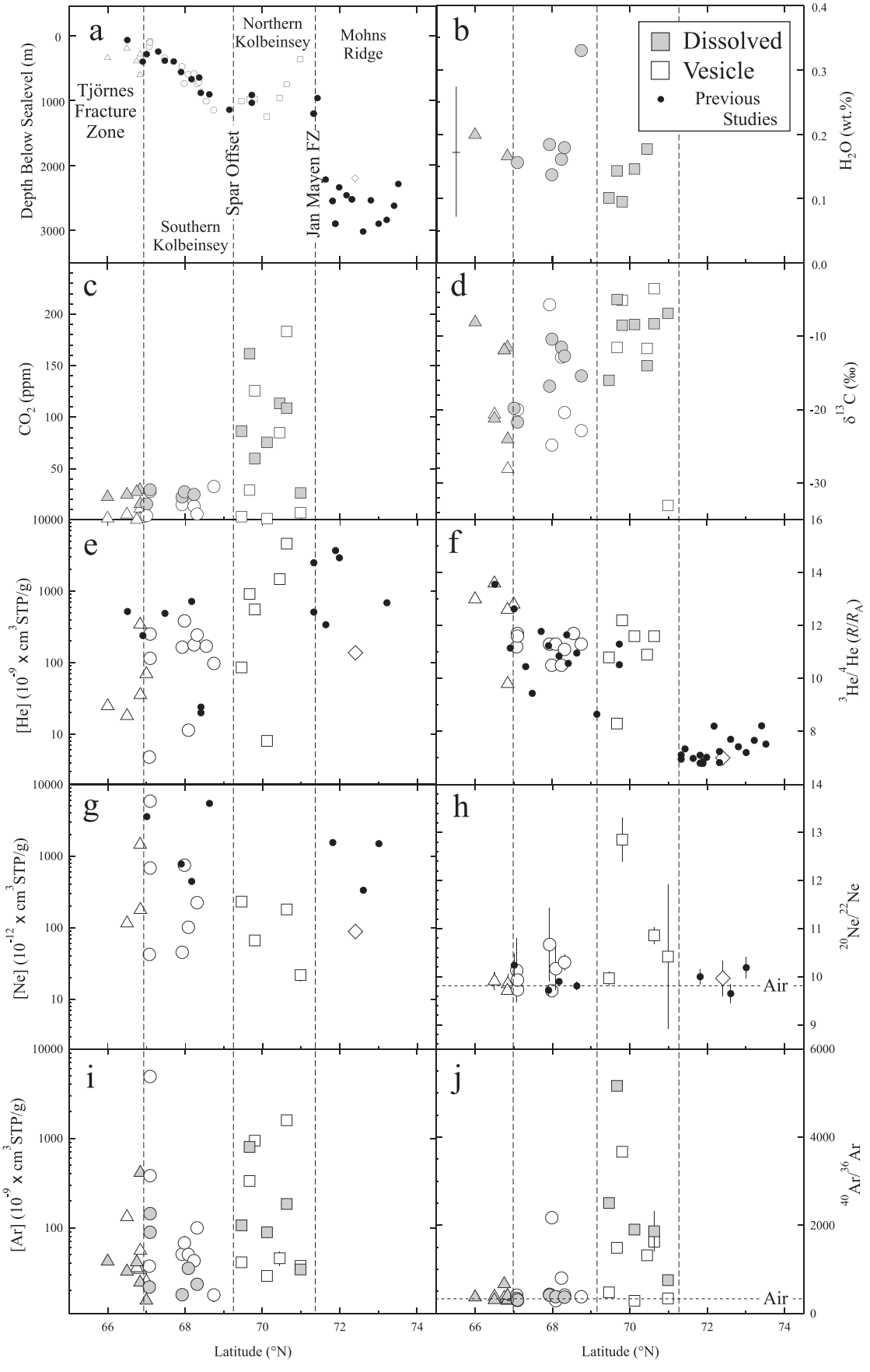
a
b
c
d
e
f
g
h
i
j
Depth Below Sealevel (m)
Tjörnes Fracture Zone
Southern Kolbeinsey
Spar Offset
Northern Kolbeinsey
Jan Mayen FZ
Mohns Ridge
Dissolved
Vesicle
Previous Studies
H2O (wt.%)
CO2 (ppm)
δ 13C (‰)
[He] (10-9 x cm3STP/g)
3He/4He (R/RA)
[Ne] (10-12 x cm3STP/g)
20Ne/22Ne
Air
[Ar] (10-9 x cm3STP/g)
40Ar/36Ar
Air
Latitude (°N)
Latitude (°N)

Figure 2

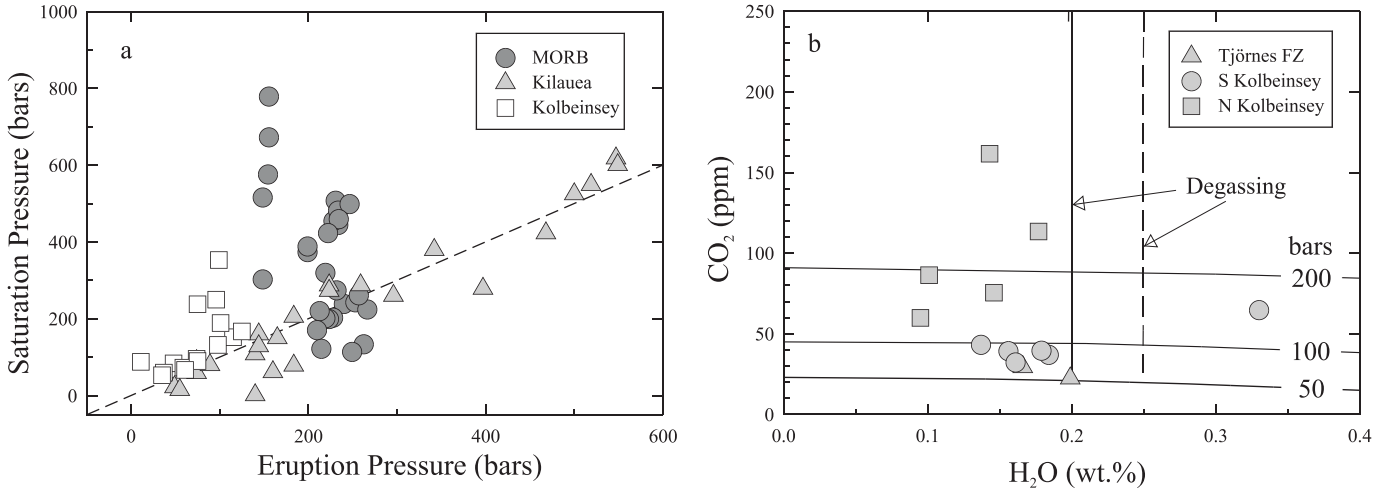
a
MORB
Kilauea
Kolbeinsey
Saturation Pressure (bars)
Eruption Pressure (bars)
0
200
400
600
800
1000
b
Tjörnes FZ
S Kolbeinsey
N Kolbeinsey
Degassing
bars
200
100
50
CO_2 (ppm)
H_2O (wt.%)
0.0
0.1
0.2
0.3
0.4
50
100
150
200
250

Figure 3

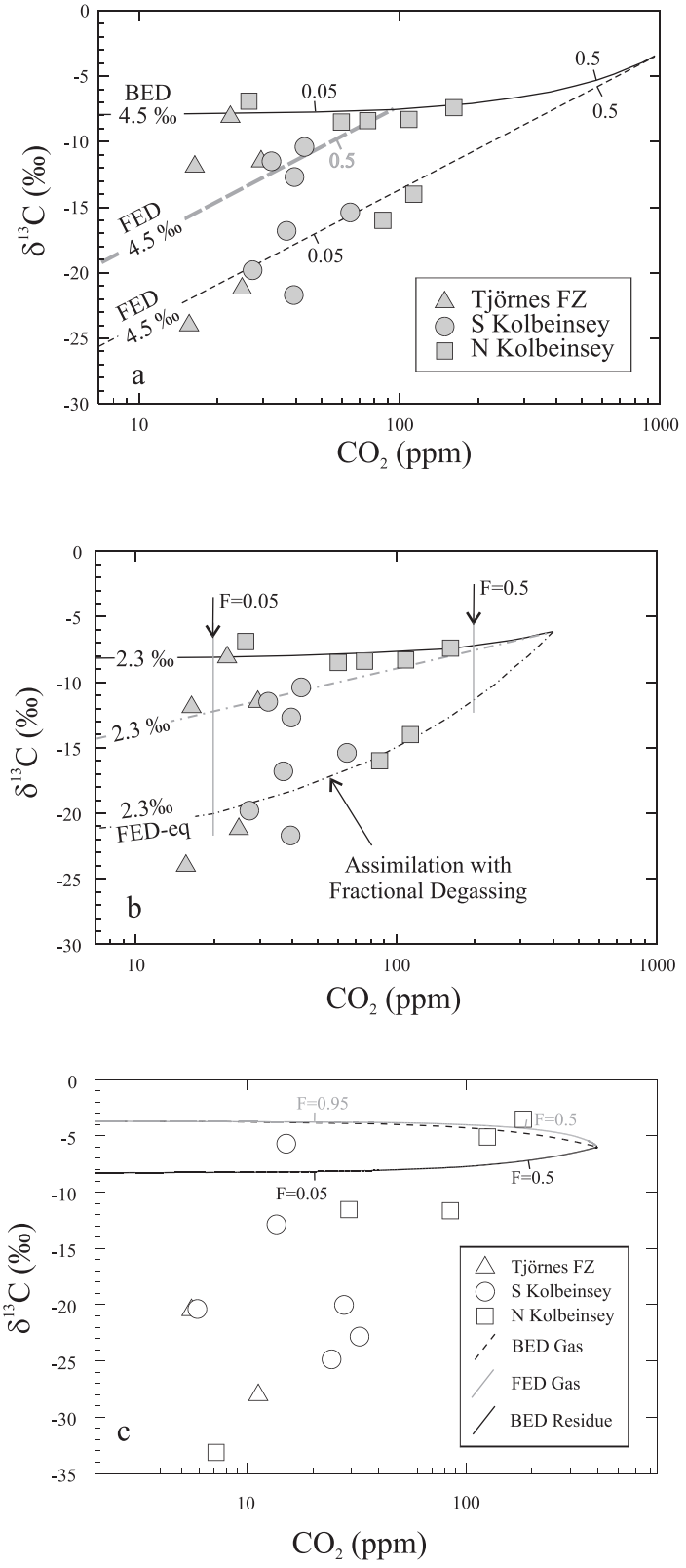
BED
4.5 ‰
0.05
0.5
0.5
FED
4.5 ‰
0.5
0.05
FED
4.5 ‰
Tjörnes FZ
S Kolbeinsey
N Kolbeinsey
a
δ13C (‰)
CO2 (ppm)
F=0.05
F=0.5
2.3 ‰
2.3 ‰
2.3‰
FED-eq
Assimilation with
Fractional Degassing
b
δ13C (‰)
CO2 (ppm)
F=0.95
F=0.5
F=0.5
F=0.05
Tjörnes FZ
S Kolbeinsey
N Kolbeinsey
BED Gas
FED Gas
BED Residue
c
δ13C (‰)
CO2 (ppm)

Figure 4

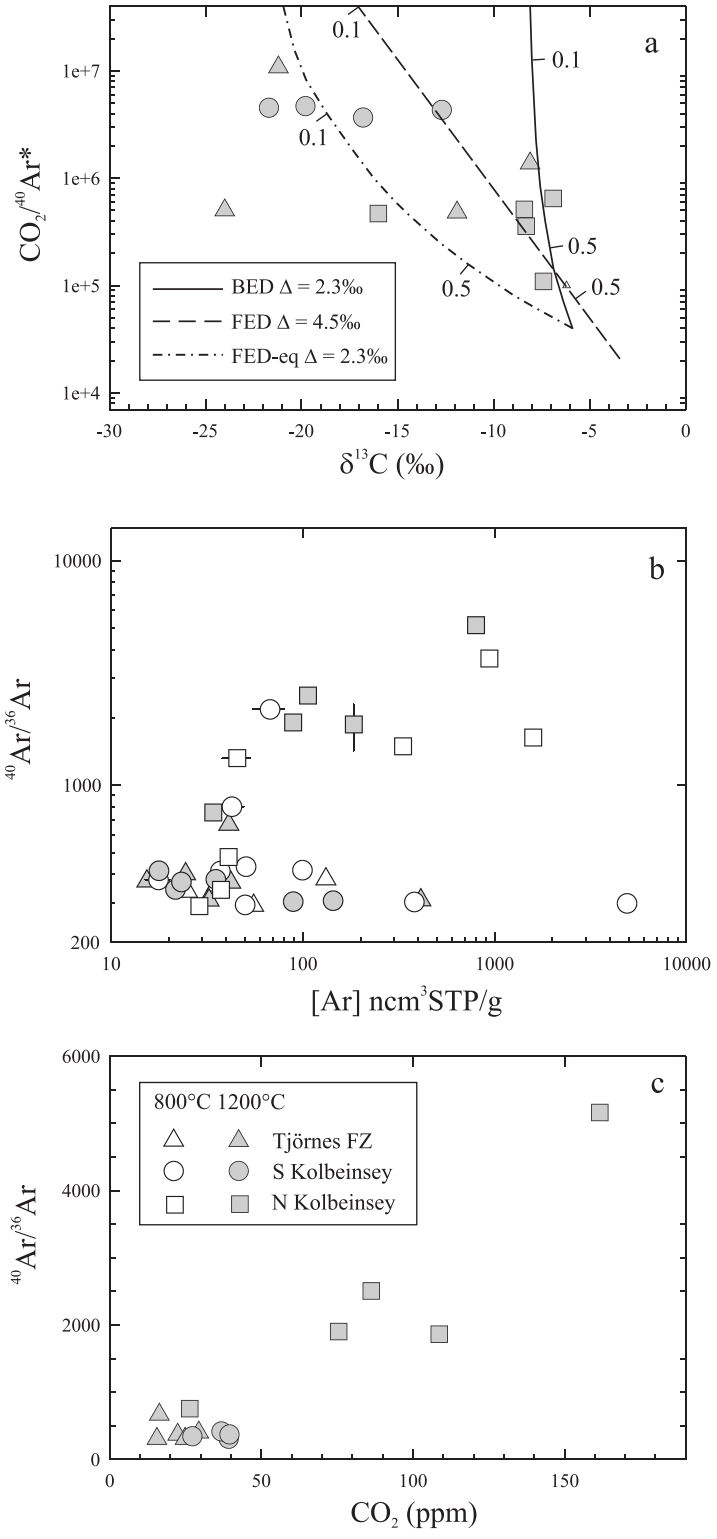
a
0.1
0.1
0.1
0.5
0.5
0.5
BED Δ = 2.3‰
FED Δ = 4.5‰
FED-eq Δ = 2.3‰
1e+7
1e+6
1e+5
1e+4
-30
-25
-20
-15
-10
-5
0
CO2/40Ar*
δ13C (‰)
b
10000
1000
200
10
100
1000
10000
40Ar/36Ar
[Ar] ncm3STP/g
c
800°C 1200°C
Tjörnes FZ
S Kolbeinsey
N Kolbeinsey
6000
4000
2000
0
0
50
100
150
40Ar/36Ar
CO2 (ppm)

Figure 5

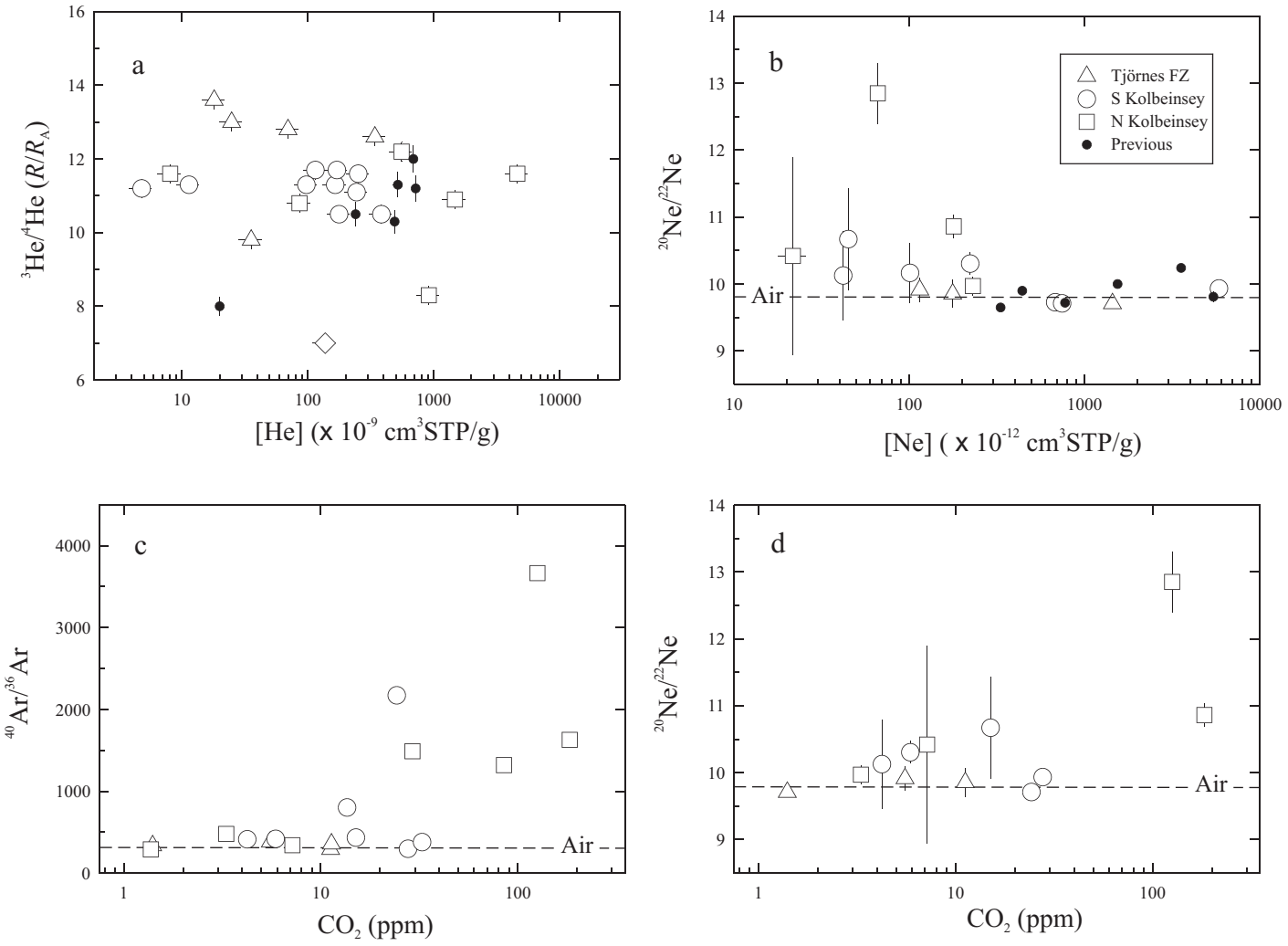
a
$^3He/^4He$ (R/R_A)
[He] (x 10^{-9} cm^3STP/g)
b
Tjörnes FZ
S Kolbeinsey
N Kolbeinsey
Previous
Air
$^{20}Ne/^{22}Ne$
[Ne] (x 10^{-12} cm^3STP/g)
c
$^{40}Ar/^{36}Ar$
Air
CO_2 (ppm)
d
$^{20}Ne/^{22}Ne$
Air
CO_2 (ppm)

Figure 6

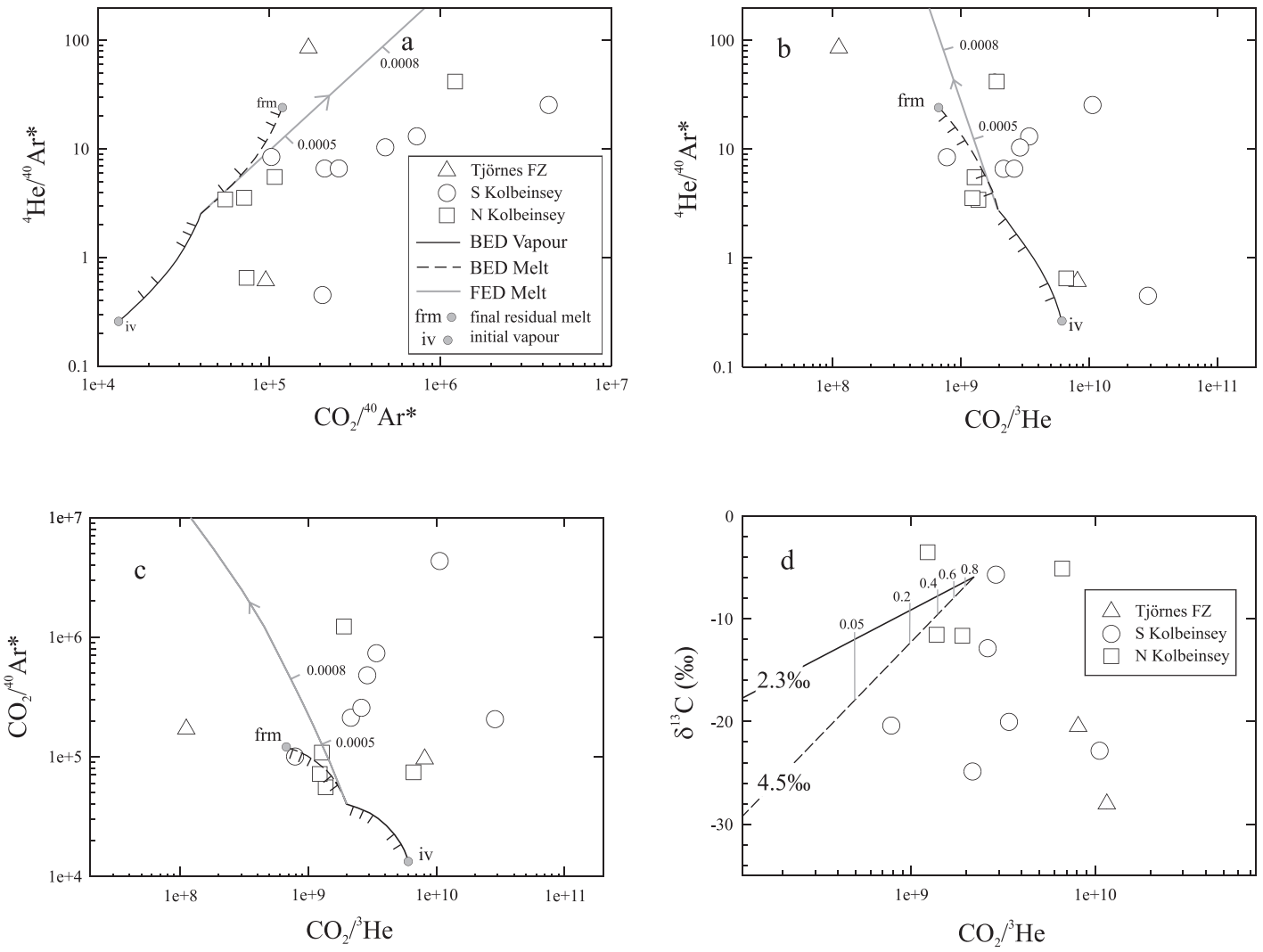
a
b
c
d
0.0008
0.0005
frm
iv
Tjörnes FZ
S Kolbeinsey
N Kolbeinsey
BED Vapour
BED Melt
FED Melt
final residual melt
initial vapour
$^4He/^{40}Ar^*$
$CO_2/^{40}Ar^*$
$CO_2/^3He$
$\delta^{13}C$ (‰)
0.05
0.2
0.4
0.6
0.8
2.3‰
4.5‰

Figure 7

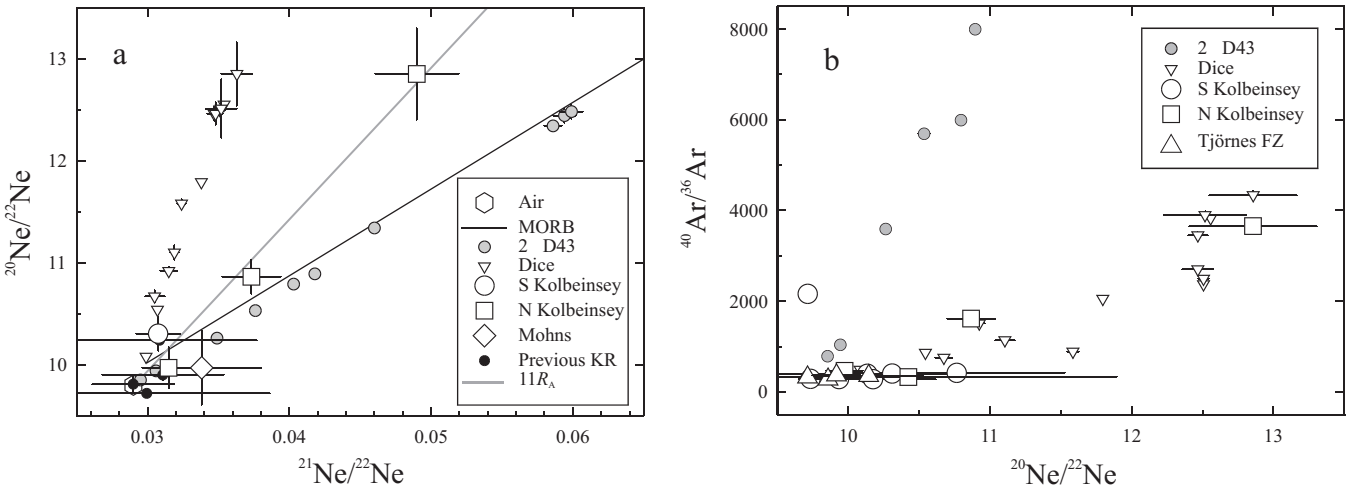
a
b
Air
MORB
2 D43
Dice
S Kolbeinsey
N Kolbeinsey
Mohns
Previous KR
11R_A
Tjörnes FZ
^{20}Ne/^{22}Ne
^{21}Ne/^{22}Ne
^{40}Ar/^{36}Ar

Figure 8

Table 1. Location, depth and CO_2, H_2O and He analytical data for Kolbeinsey Ridge and Tjörnes Fracture Zone glasses.

				Dissolved		Vesicle		Total	Crush		
Sample	Latitude (°N)	Longitude (°W)	Depth (m)	CO_2 (ppm)	$\delta^{13}C$ (‰)	CO_2 (ppm)	$\delta^{13}C$ (‰)	H_2O (wt.%)	Weight (mg)	[He] 10^{-9}xcm^{-3}STP/g	$^3He/^4He$ (xR_A)
Tjörnes Fracture Zone											
Pos1096A	66.001	18.704	346	22.4	-8.1	11.3	-28.1	0.20	75	24.9	13.0
Pos1117A	66.500	17.301	201	24.9	-21.2				85	18.1	13.6
Pos1105B	66.753	18.091	397	16.4	-11.9	1.4					
Pos1093	66.839	18.708	610	29.4	-11.5	1.7		0.17	90	342.2	12.6
Pos1091A	66.844	18.116	290	15.6	-24.0	5.6	-20.6		92	35.6	9.8
Pos1094B	67.001	18.664	285						82	69.8	12.8
South Kolbeinsey											
Pol37DS-1	67.007	18.747	170	27.3	-19.8	4.3			166	4.8	11.2
Pol25Ds-2a	67.095	18.738	91						82	115.2	11.7
Pol22Ds-2a	67.096	18.722	110	39.2	-21.7	27.7	-19.9	0.16	208	251.7	11.6
Pos0002/2	67.925	18.362	479	36.9	-16.8	15.0	-5.8	0.18	214	165.3	11.3
Pos404-1	67.983	18.307	741	43.1	-10.4	24.2	-24.8	0.14	95	384.2	10.5
Pos457-1	68.085	18.237	601						90	11.4	11.3
Pos447-1	68.232	18.177	590	32.2	-11.5	13.5	-12.7	0.16	85	177.6	10.5
Pos446-1	68.311	18.082	748	39.5	-12.7	5.9	-20.3	0.18	86	244.3	11.1
Pos438-2	68.548	17.788	1013						94	170.6	11.7
Pos436-1	68.745	17.621	1150	64.6	-15.4	32.6	-22.8	0.33	94	97.6	11.3
North Kolbeinsey											
Pol21844	69.463	15.946	1014	86.3	-16.0	3.3		0.10	82	86.2	10.8
Pol21847	69.996	15.552	986	161.6	-7.4	29.1	-11.9	0.14	297	915.8	8.3
Pol21848	69.804	15.680	980	59.8	-8.5	125.6	-5.1	0.10	57	557.1	12.2
Pol21850	70.121	15.318	1250	75.5	-8.4	1.4		0.15	331	8.1	11.6
Pol21854	70.449	14.776	961	113.4	-14.0	85.0	-11.7	0.18	450	1476	10.9
Pol21856-3	70.631	14.519	754	108.7	-8.3	183.3	-3.4		327	4623	11.6
Pol21860B	70.988	13.984	367	26.4	-6.9	7.2	-33.2				
Mohns Ridge											
Met23288-1	72.407	1.700	2200						70	137.9	7.0

Table 2. Neon and argon stepped heating data for Kolbeinsey Ridge, Tjörnes Fracture Zone and Mohns Ridge glasses.

Sample	Temp (°C)	weight mg	[Ne] 10^{-12}xcm^{-3}STP/g	1σ	$^{21}Ne/^{22}Ne$	1σ	$^{20}Ne/^{22}Ne$	1σ	[Ar] 10^{-9}xcm^{-3}STP/g	1σ	$^{40}Ar/^{36}Ar$	1σ	$^{38}Ar/^{36}Ar$	1σ	$^{4}He/^{40}Ar^{*}$
South Kolbeinsey															
Pol37DS-1	800	143.7	42.1	4.0	*0.0320*	0.0090	*10.13*	0.66	37.2	2.3	*413.9*	11.9	0.18804	0.00100	0.45
	1200		n.r.						21.7	0.7	342.9	7.6	0.19067	0.00018	
Pol25Ds-2a	800	232.4	680.4	12.2	0.0302	0.0007	9.73	0.05	381.7	5.5	301.6	1.3	0.18951	0.00015	16.34
	1200		171.4	12.4	0.0308	0.0022	9.96	0.23	89.1	0.7	302.6	3.3	0.18686	0.00013	
Pol22Ds-2a	800	171.2	5850	44	0.0293	0.0051	9.93	0.01	4903	52	297.2	0.2	0.18686	0.00001	13.07
	1200		207.6	7.4	0.0294	0.0035	9.75	0.19	143.8	0.7	305.4	1.5	0.18791	0.00016	
Pos0002/2	800	169.5	45.0	4.8	*0.0343*	0.0113	*10.67*	0.76	50.6	2.6	433.3	10.4	0.18796	0.00070	10.34
	1200		34.0	3.7	*0.0383*	0.0138	*9.56*	0.79	17.8	0.4	415.5	11.1	0.19097	0.00084	
Pos404-1	800	220.6	745.0	11.8	0.0298	0.0006	9.71	0.03	67.5	17.6	*2173*	83	0.18831	0.00015	6.59
	1200		170.1	6.2	*0.0305*	0.0019	*9.92*	0.19	n.r.						
Pos457-1	800	127.6	101.1	6.1	0.0362	0.0054	10.17	0.45	50.1	2.6	292.8	10.2	0.18792	0.00070	
	1200		39.2	5.4	0.0365	0.0198	9.53	0.98	35.2	0.9	380.5	7.5	0.18943	0.00032	
Pos447-1	800	183.2	n.r.						42.7	7.5	801.6	38.5	0.18959	0.00080	6.60
Pos446-1	800	172.7	222.6	7.0	0.0307	0.0015	10.30	0.17	99.6	4.1	418.0	7.7	0.19343	0.00011	8.43
	1200		n.r.						23.3	0.5	370.4	17.7	0.18846	0.00273	
Pos436-1	800	175.3	n.r.						17.7	2.6	*378.4*	33.0	0.18950	0.00080	25.39
Mohns Ridge															
Met23288-1	800	185.4	88.1	5.1	*0.0338*	0.0042	*9.97*	0.36	n.r.						

n.r. Gas yield not resolved from blank.

Table 2 cont.

Sample	Temp (°C)	weight mg	[Ne] 10^{-12}xcm^{-3}STP/g	1σ	$^{21}Ne/^{22}Ne$	1σ	$^{20}Ne/^{22}Ne$	1σ	[Ar] 10^{-9}xcm^{-3}STP/g	1σ	$^{40}Ar/^{36}Ar$	1σ	$^{38}Ar/^{36}Ar$	1σ	$^{4}He/^{40}Ar^{*}$
North Kolbeinsey															
Pol21844	800	220.1	231.0	6.5	0.0315	0.0013	9.97	0.13	41.1	2.8	*478.7*	14.8	0.18755	0.00150	5.52
	1200		68.3	4.1	*0.0343*	0.0050	*10.09*	0.43	106.5	3.7	2506	13	0.18994	0.00089	
Pol21847	800	174.6	n.r.						333.6	4.6	1490	8	0.18877	0.00040	3.43
	1200		n.r.						801.1	5.4	5160	20	0.18771	0.00045	
Pol21848	800	256.0	66.2	5.7	0.0490	0.0029	12.85	0.45	939.7	27.9	3667	10	0.18697	0.00040	0.65
Pol21850	800	220.3	n.r.						28.9	2.2	289.3	15.4	0.18870	0.00120	
	1200		n.r.						89.1	3.3	1903	15	0.18917	0.00117	
Pol21854	800	203.0							45.6	7.8	*1320*	48	0.18885	0.00200	41.78
Pol21856-3	800	230.2	179.5	5.7	0.0373	0.0021	10.86	0.17	1592	24	1629	4	0.18945	0.00025	3.55
	1200		606.7	10.9	0.0302	0.0007	9.73	0.05	184.6	1.8	1863	443	0.19283	0.00418	
Pol21860B	800	167.7	21.7	3.9	*0.0329*	0.0294	*10.42*	1.47	37.5	2.0	*341.6*	10.4	0.18794	0.00075	
	1200		26.1	7.2	0.0354	0.0204	10.53	1.14	34.2	0.9	756.0	10.4	0.18971	0.00083	
Tjörnes F.Z.															
Pos1091A	800	157.8	177.1	7.9	0.0319	0.0021	9.85	0.20	55.5	2.5	291.0	7.6	0.18680	0.00040	
	1200		883.0	14.0	0.0298	0.0006	9.86	0.04	413.0	9.1	307.8	0.6	0.18797	0.00014	
Pos1094B	800	184.8							25.1	1.4	*335.9*	11.5	0.18773	0.00095	23.45
	1200		21.5	2.7	*0.0397*	0.0189	*9.81*	0.91	15.4	0.5	373.3	8.2	0.19192	0.00067	
Pos1093	800	180.3	1445	17	0.0296	0.0003	9.71	0.01	34.0	0.5	335.9	2.1	0.18785	0.00055	85.00
	1200		109.2	1.8	0.0312	0.0007	9.59	0.05	24.5	0.2	402.2	3.0	0.18889	0.00042	
Pos1096A	1200	195.5	50.1	3.1	*0.0317*	0.0045	*10.14*	0.38	42.1	0.4	369.1	2.8	0.18826	0.00030	
Pos1105B	800	180.4	n.r.						35.5	2.9	*358.2*	9.1	0.18819	0.00060	
	1200		n.r.						41.2	1.1	667.6	6.0	0.18795	0.00046	
Pos1117A	800	231.3	114.9	3.9	0.0317	0.0017	9.91	0.18	132.0	2.7	381.7	2.2	0.18894	0.00020	0.61
	1200		75.9	3.2	*0.0305*	0.0024	*9.67*	0.26	32.5	0.7	307.1	2.8	0.18927	0.00024	

Appendix 1

Results of CO_2 extraction from Kolbeinsey Ridge and Tjörnes Fracture Zone basaltic glass by stepped heating at Scripps Institution of Oceanography. CO_2 yields are in ng of carbon and $^{13}C/^{12}C$ ratios are reported in the δ notation relative to V-PDB. All data for unknowns are corrected for presence of a blank.

Sample	weight	400°C		600°C		700°C		800°C		900°C		1000°C		1100°C		1200°C	
	mg	ng C	$\delta^{13}C$	ng C	$\delta^{13}C$	ng C	$\delta^{13}C$	ng C	$\delta^{13}C$	ng C	$\delta^{13}C$	ng C	$\delta^{13}C$	ng C	$\delta^{13}C$	ng C	$\delta^{13}C$
South Kolbeinsey																	
37DS-1	130.2	768	n.d.	301	n.d.	83	n.d.	49	n.d.	20	n.d.	n.r.	n.d.	249	c.o.	720	-19.8
22DS2a	132.03	309	n.d.	162	n.d.	303	c.o.	574	c.o.	119	-19.9	267	c.o.	524	c.o.	623	-21.7
Pol0002/2	131.14	841	n.d.	485	n.d.	141	c.o.	396	-5.8	n.r.	n.d.	289	c.o.	487	c.o.	542	-16.7
404-1	108.06	511	n.d.	2585	-25.7	237	c.o.	283	c.o.	194	-24.8	275	c.o.	261	c.o.	736	-10.4
447-1	112.24	1419	n.d.	160	n.d.	n.r.	n.d.	414	-12.7	n.r.	n.d.	192	c.o.	83	c.o.	712	-11.5
446-1	107.14	1136	n.d.	416	n.d.	30	c.o.	111	c.o.	30	-20.0	160	c.o.	255	c.o.	740	-12.7
436-1	105.8	952	n.d.	196	n.d.	293	c.o.	273	c.o.	374	-22.8	685	c.o.	879	-15.2	299	-16.5
North Kolbeinsey																	
21844	116.13	673	n.d.	192	n.d.	69	n.d.	14	n.d.	22	n.d.	768	c.o.	667	c.o.	1298	-16.0
21847	99.5	734	n.d.	105	n.d.	89	c.o.	366	c.o.	336	-11.9	487	c.o.	293	-8.2	3606	-7.3
21848	98.98	4999	-30.8	404	n.d.	2729	c.o.	621	-5.1	40	n.d.	267	c.o.	146	c.o.	1203	-8.5
21850	115.7	97	n.d.	18	n.d.	24	n.d.	18	n.d.	n.r.	n.d.	501	c.o.	261	-10.1	1621	-7.6
21854	101.02	560	n.d.	297	n.d.	457	n.d.	1536	c.o.	350	-11.7	910	c.o.	499	c.o.	1714	-14.0
21856-3	99.96	5391	c.o.	1512	-31.9	1170	c.o.	3776	-4.9	51	c.o.	463	c.o.	299	-9.9	2201	-7.8
21860B	117.26	796	n.d.	206	n.d.	0	n.d.	91	c.o.	139	-33.2	57	c.o.	53	c.o.	736	-6.9
Tjörnes Fracture Zone																	
1091A	85.6	1003	n.d.	291	n.d.	95	c.o.	97	c.o.	71	-28.1	83	c.o.	127	c.o.	154	-24.0
1093	126.56	9640	c.o.	53	-29.0	34	n.d.	12	n.d.	n.r.	n.d.	160	c.o.	168	c.o.	687	-11.4
1096A	114	865	n.d.	259	n.d.	20	n.d.	32	n.d.	n.r.	n.d.	170	c.o.	158	c.o.	370	-8.1
1105B	118.57	716	n.d.	245	n.d.	n.r.	n.d.	n.r.	n.d.	368	-15.6	n.r.	n.d.	n.r.	n.d.	530	-11.9
1117A	145.22	1207	n.d.	524	n.d.	71	c.o.	77	c.o.	73	-20.6	n.r.	n.d.	146	c.o.	839	-21.2
Mean Blank		103	n.d.	73	n.d.	49	c.o.	63	c.o.	53	-26.6	34	n.d.	42	c.o.	30	-26.8

n.r. CO_2 yield not resolved from blank.
n.d. not determined.
c.o. gas combined with following step(s) for isotopic analysis.